

REVIEWS OF TOPICAL PROBLEMS

PACS numbers: **02.70.–c**, **92.60.–e**, 96.30.Ea, 96.30.Gc

Escape of planetary atmospheres: physical processes and numerical models

V I Shematovich, M Ya Marov

DOI: https://doi.org/10.3367/UFNe.2017.09.038212

Contents

Abstract. We address the problem of the dissipation (escape) of planetary atmospheres and discuss the physical mechanisms controlling the nature of the relevant processes and review the mathematical models and numerical methods used in the analysis of this phenomenon, taking the limitations imposed by available experimental data into account. The structural and dynamic features of the aeronomy of Earth and terrestrial planets are discussed in detail; they are key in determining the energy absorption rate and the atmosphere escape rate. A kinetic Monte Carlo method developed by the authors for investigating the thermal and nonthermal processes of atmospheric escape is presented. Using this approach and spacecraft data, atomic loss rates from the Venusian and Martian atmospheres via a variety of escape processes are estimated, and their role at the current and early evolutionary stages of these planets is discussed. The discovery of exosolar planets, model studies of the dissipation of their gas envelopes, and the likely impact of the dissipation mechanisms on the planetary atmosphere and climate evolution have stimulated the study of this field and made it a topical research subject.

V I Shematovich Institute of Astronomy, Russian Academy of Sciences, ul. Pyatnitskaya 48, 119017 Moscow, Russian Federation
E-mail: shematov@inasan.ru
M Ya Marov Vernadsky Institute of Geochemistry and Analytic Chemistry, Russian Academy of Sciences, ul. Kosygina 19, 119991 Moscow, Russian Federation
E-mail: marovmail@yandex.ru

Received 28 March 2017, revised 15 September 2017
Uspekhi Fizicheskikh Nauk **188** (3) 233 – 265 (2018)
DOI: https://doi.org/10.3367/UFNr.2017.09.038212
Translated by M Zh Shmatikov; edited by A M Semikhatov

Keywords: planetary atmosphere, aeronomy, modeling, suprathermal atoms, thermal and nonthermal escape processes, kinetic Monte Carlo method, exoplanets

1. Introduction

Studies of the evolution of atmospheres of Solar System planets and planetary systems of other stars have significantly advanced during recent decades. Progress has been achieved owing to unique measurement data obtained by spacecraft during their flights to different objects in the Solar System, observations of the outer bodies of the solar system and exoplanets using space and ground-based telescopes, and the development of mathematical simulation methods. These results have shaped a new basis for the physics of the upper atmosphere, i.e., the aeronomy that is directly linked to planetary cosmogony. In particular, they have allowed drawing a conclusion that dissipation of a planetary atmosphere (or atmospheric escape) plays an important role in the evolution of planets primarily of terrestrial planets of the Solar System, although many details of those events are not fully clear and remain the topic of active discussions [1–3].

Two main regions are distinguished in the upper atmosphere: the thermosphere and the exosphere; within them, there is also the ionosphere, which contains electrons and ions of various compositions and densities. The thermosphere is limited from below by the homopause (altitudes of 115 to 130 km), above which the contribution of turbulent (eddy) mixing is small and the altitude distribution of its main species has its own (partial) scales heights of a homogeneous atmosphere (see below). Due to direct absorption of solar short-wave radiation by the rarefied gas, the temperature in the thermosphere increases above the minimum temperature of the upper boundary of the mesosphere lying below (mesopause). In addition to heating by solar extreme ultraviolet (UV) radiation, the structure and dynamics of the thermosphere are also governed by infrared (IR) heating in its lower layers, radiation and collision cooling, dissipation of the energy of gravitational and planetary waves, thermal tides, and precipitation of charged particles. Particle collisions occur in the thermosphere, while in the exosphere, which is located higher (and is also referred to as the planetary corona), collisions are virtually absent. The exosphere is separated from the thermosphere by the exobase, above which atoms and molecules may run planet-size distances with a very low probability of collision. At such altitudes, particles whose energy is higher than the gravitational attraction energy and which run along ballistic trajectories in the radial direction, can escape into open space. The exobase is defined as the altitude h_e at which the atmospheric hight scale becomes comparable to the characteristic microscopic scale, i.e., the mean free path between collisions (for a more detailed definition, see Section 2). For Earth, $h_e \sim 500$ km, while for Mars and Venus h_e ranges from 160 to 200 km. Accordingly, above the exobase, the number of particle collisions is very limited and, from the standpoint of the kinetic gas theory, any particle in this zone may leave the planet's atmosphere.

A high velocity at the altitude h_e can be reached in a number of physical processes, determined primarily by the temperature of the upper atmosphere at those altitudes, which given rise to thermal escape; we note that the fraction of the particles leaving the atmosphere depends on the local temperature, which has spatial and temporal variations. If the atmosphere near the exobase is in hydrostatic equilibrium, the local velocity distribution of particles is described by the Maxwell distribution and the process is referred to as the Jeans escape (or evaporation of the atmosphere), and the ratio of the gravitational and kinetic energies of particles at this level is called the Jeans escape parameter. If this parameter is close to unity, the planet's gravity weakly binds its atmosphere. The state of the latter deviates from hydrostatic equilibrium and the local velocity distribution of particles is described by the Maxwell distribution with a velocity shift that increases the probability of particle escape. This escape scenario is usually referred to as hydrodynamic outflow or planetary wind, in analogy to solar wind. In both cases just discussed, the escape regime is determined by the temperature of the upper atmosphere. Therefore, both Jeans and hydrodynamic escape are particular cases of thermal escape. More specifically, in the case of Jeans escape, the atmosphere dissipation does not alter the velocity distribution of particles (the temperature of the upper atmosphere) at the level h_e, while in the case of hydrodynamic escape, this regime *itself* strongly affects the velocity distribution of particles and the temperature of the upper atmosphere. A detailed description of the thermal dissipation, the history of exploration of those processes, and the modern state of studies can be found in popular reviews [2, 3].

In addition to the thermal dissipation mechanism, there are nonthermal mechanisms of the planetary atmosphere escape, wherein the velocity of escape particles does not depend on the exobase temperature. The major part of nonthermal escape processes are related to exothermal reactions of atmospheric photochemistry, the availability of ions, and their behavior in electric and magnetic fields [1, 2]. The efficiency of this mechanism depends on the body where it occurs: photochemical escape proved to be of uttermost importance for Mars, while it is much less efficient for Earth and super-Earths among the exoplanets. This difference occurs because the maximum kinetic energy of an oxygen atom gained in the reaction of dissociative recombination of O_2^+ does not exceed several electron-volts, which is significantly smaller than the escape energy for a planet more massive than Mars. The nonthermal escape can have an impact on switching the upper atmospheres of planets from the hydrostatic regime to the hydrodynamic one if, for example, the charge exchange between the planetary corona gas and the stellar wind plasma is taken into account. Updated estimates of the relative importance of thermal and nonthermal escape for the terrestrial planets of the Solar System are presented in recent reviews [2, 3].

Currently, studies of the physical and chemical dissipation of planetary atmospheres are stimulated by the rapid growth in the number of exoplanets, whose observations enable shaping a new basis for planetary cosmogony (in particular, studying the evolution of those planets using state-of-the-art models of atmospheric escape). An analysis of observations and results of simulation of exoplanet atmospheres under the effect of host stars shows, in particular, that a planet has been created, the primordial atmosphere outflows as a result of absorption and heating of the atmosphere by extreme UV radiation of the star in the wavelength range 1–100 nm [4]. As the UV radiation flux becomes weaker, the atmosphere loss regime changes from hydrodynamic expansion of the thermosphere to 'evaporation' in a hydrostatic regime. In the process of that transition, the onset of various nonthermal processes occurs, which make a significant contribution to overall atmospheric losses. As the flux of extreme UV radiation from a young and active star diminishes to a moderate value (approximately less than one fifth of the present-day flux of hard solar UV radiation) in the case where gaseous CO_2 or N_2 become the main species in the atmosphere, all dissipation processes increase atmospheric losses, although the impact on the state of the atmosphere is significantly smaller than or inessential compared to the effect of those processes during the early active UV phase of the young star.

Observation and simulation of the evolution of the atmospheres of exoplanets are of importance for understanding the processes that may have occurred on the terrestrial planets of the Solar System and, primarily, on Earth. Figure 1 shows possible scenarios of the formation of Earth's early atmosphere according to [4, 5]. After collisional (catastrophic) outgassing, the hot vapor atmosphere is subject to a strong flux of extreme UV radiation from the young Sun, resulting in the formation of an extended hydrogen exosphere due to dissociation of H_2O molecules. In comparison with insolation on Venus, which orbits closer to the Sun, insolation on Earth was weaker, and hence the atmosphere faster approached the state in which the remaining water vapor could condense to create the terrestrial water ocean. CO_2 molecules presumably precipitated from the atmosphere and were bound in the lithosphere as carbonates

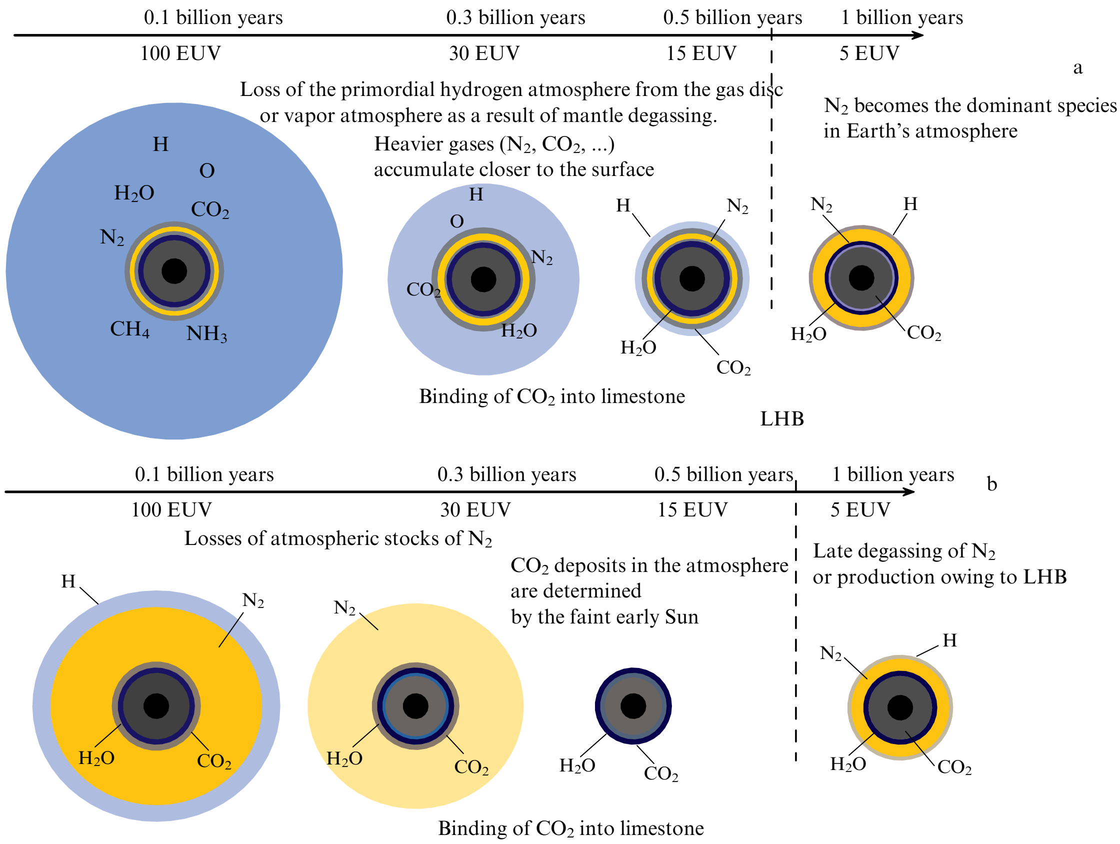

Figure 1. Possible scenarios of the formation of Earth's early atmosphere (from [5]). (a) Accumulation of the initial primordial atmosphere owing to the accretion of H_2 molecules from the gas disc. (b) Production of H_2O, CO_2, N_2, NH_3, CH_4, ... vapors owing to degassing of the mantle by EUV (extreme ultraviolet) radiation; LHB is late heavy bombardment. The age of the star and the planet and the activity of the star in the EUV radiation range with time (in comparison to the present-day activity of the Sun) are shown with an arrow (from left to right).

(limestone), while nitrogen was released into the atmosphere as a result of denitrification, to gradually become the main gas component. In addition to the release of gases from rocks also as a result of volcanic activity, volatile species could also be added to the atmosphere during the period of late heavy bombardment (LHB) from the outer regions of the Solar System.

It is generally assumed (see, e.g., [5]) that for all the terrestrial planets in the Solar System, the temporal scales of the loss of primordial atmospheres captured from the protosolar nebula at the formation stage were relatively short. Afterwards, they followed different evolutionary paths. Venus probably rapidly lost oceans owing to an irreversible greenhouse effect and atmospheric escape due to its closeness to the Sun. As a result, its average atmosphere grew more humid, which favored the UV dissociation of water vapor accompanied by the escape of hydrogen from the atmosphere [6–9]. The concentration of hydrogen could partly affect the climate of early Earth, because the collision-induced absorption of solar radiation by hydrogen and nitrogen could provide additional heating to the atmosphere and thus to resolve the 'paradox of early Earth', the occurrence of a low temperature (some 30° lower than the triple point of water) near the surface, owing to weak solar luminosity [10]. The answer to the question of whether Earth preserved a hydrogen-enriched atmosphere in the Archean also essentially depends on the atmospheric escape model [11, 12]. Unfortunately, to date, this problem has not been studied satisfactorily. As an alternative to the hydrogen-enriched atmosphere of early Earth, a dense carbon-dioxide atmosphere and an atmosphere with a significant content of methane have been conjectured. Both CO_2 and CH_4 are greenhouse gases, and both models can in principle provide a temperature close to Earth's surface that exceeds the equilibrium temperature by several dozen degrees and thus solve the paradox of the young Sun. However, the issue of the source and content of those gases on early Earth remains open and, moreover, in the case of a dense carbon-dioxide atmosphere, 'transparency windows' remain for the outgoing IR radiation; to 'close' those windows, an admixture of other gases, for example, water vapor or sulfur-containing gases, is needed [9, 13].

In a number of studies, a similar model approach is applied to Mars. It is assumed that during its history, the planet had a dense (an order of magnitude denser than the current one) warm and humid atmosphere that dates to the transition between the so-called Noachian and Hesperian time periods ($\sim 4-3.6$ billion years ago), the predecessors of the contemporary Amazonian period of cold and dry Mars [14]. For early Mars to be warm and humid, it is assumed that it had a dense CO_2 atmosphere [15]. In line with the proposed effect of the absorption of radiation induced by H_2–CO_2 collisions, causing an increase in the surface temperature to a value above the freezing point, a combination of two factors — partial CO_2 pressure over 2 bars and a concentration of hydrogen greater than 10% in the gas mixture — is needed. In the case of volcanic activity, to cause even a short-time warming, the partial pressure of

CO_2 is to be no less than 1 bar [17]. A recent study [18] showed that if even a small amount of methane (the second most efficient greenhouse gas after CO_2) is added to a rarefied carbon-dioxide atmosphere, the greenhouse effect is greatly enhanced, resulting in an increase in the temperature by several dozen degrees if the CH_4 concentration only increases by one percent. In other words, if the early atmosphere of Mars had been as dense as Earth' atmosphere, the temperature of Mars's surface would be close to the surface temperature of present-day Earth for a methane concentration as low as 2% to 10%. We note that if Mars had been formed from planetesimals similar to those from which Earth and Venus were formed, it would have had a primordial CO_2 atmosphere with a surface pressure over 10 bar; this, however, disagrees with the known isotope ratios for terrestrial planets and carbonaceous chondrites [19]. However, even if this were the case, Mars's mass is only one tenth of Earth's mass, and therefore it could hardly have had a CO_2 atmosphere with a pressure over 1 bar in the early Noachian period [20]. At the same time, a factor that favors retaining a sufficiently dense atmosphere is that the atmospheric losses of Mars during the Noachian and Hesperian periods with low Sun luminosity were relatively small [20].

Addressing Venus, we note that regardless of whether Venus had a primordial ocean, each of the evolutionary scenarios results in developing a run-away greenhouse effect and present-day climatic conditions of a hot and dense atmosphere. However, as in the case of Mars, it cannot be ruled out that at the very early stages of its evolution, Venus featured a more temperate climate. The corresponding model assumes the existence of a negative feedback loop that stabilized some equilibrium prior to switching to a positive feedback that resulted in a temperature increase due to the run-away greenhouse effect. The negative feedback could in principle be due to a different nature of interaction between the atmosphere and the lithosphere, which is controlled by the carbonate–silicate cycle, and to the occurrence in the atmosphere of a humidity threshold (a kind of 'cold trap') under the conditions of a lower influx of solar heat from the young Sun [9]. This relation could be maintained until the Sun moved to the main sequence in the Hertzsprung–Russel diagram and its luminosity increased by about 30%. The mechanism underlying this scenario was called the 'humid greenhouse effect'. Calculations show that switching from the humid greenhouse effect to the run-away one would not have occurred if the increase in the planetary albedo to its current value owing to the formation of strong cloud cover had occurred prior to the growth in Sun's luminosity and thus balanced the increase in the solar energy flux. If this had been the case, Venus would have had a humid carbon-dioxide atmosphere with a pressure near the planet's surface of no more than several atmospheres and the temperature less than 100 °C. Consequently, the atmosphere dissipation conditions would have been different and, in particular, it would not be necessary to find a mechanism for the escape of a huge number of hydrogen atoms in the process of evaporation of the ancient ocean and, concurrently, a mechanism for evacuating oxygen atoms from the atmosphere, the thermal dissipation of which is not possible. To circumvent this difficulty, a mechanism of blow-off-assisted escape was proposed [21].

Thus, observations and theoretical models of the atmospheres of exoplanets that are subject to extreme fluxes of extreme radiation from a host star provide a nice opportunity to verify our theoretical understanding of those key processes, i.e., the thermal and nonthermal dissociation that affect the evolution of both the planet and its atmosphere, in particular, Earth and its atmosphere, at their early stages. Hopefully, future observations of exoplanets will yield stronger restrictions and will allow improving models of atmosphere dissipation, while application of those models [4] will enable us to better explain the formation of the paleoclimate and evolution of the terrestrial planets of the Solar System.

Nonthermal escape processes are naturally divided into two main categories, depending on the charge of a specific atom or molecule they have when attaining the escape energy on a trajectory that does not cross collisional areas of the atmosphere. These two categories are the escape of neutral particles and the escape of ions. However, these categories are not fully separated: a neutral particle with an energy sufficient to escape may be ionized and registered by measurement instruments as an escaping ion. The rates of loss of the planetary atmosphere owing to the escape of ions can be measured by plasma devices of spacecraft; owing to this, the models of the losses of the planetary atmosphere due to escape and outflow of ions can be verified and refined. However, if a planetary atmosphere is lost due to the escape of neutral atoms and molecules, direct measurements of escape fluxes are lacking. Therefore, to assess the rate of losses of a neutral planetary atmosphere, mathematical models have to be developed for this class of aeronomic problems [1–3]. Currently, only fluxes of energetic neutral atoms (ENAs) can be measured using ENA detectors installed on spacecrafts. Most of those detectors [ASPERA-3 (Analyzer of Space Plasma and Energetic Atoms 3) installed on the European Space Agency's Mars-Express spacecraft, MIMI (Magnetospheric Imaging Instrument) and INCA (Ion and Neutral Content Analyzer) on NASA's Cassini spacecraft, SWIA (Solar Wind Ion Analyzer) on NASA's MAVEN (Mars Atmosphere and Volatile EvolutioN), etc.] can measure ENA spectra and fluxes in the energy range above several dozen electron-volts, i.e., the spectra and fluxes of super-thermal neutral particles that are generated due to the charge exchange of ions of magnetospheric plasma and/or solar wind in the process of interaction with thermal atoms from the planetary exosphere. In other words, direct measurements of the escape fluxes of neutral particles in the range of suprathermal energies (< 10 eV) that determine the atmosphere loss rate due to nonthermal escape of atoms and molecules are currently virtually lacking.

The aim of this review is to discuss the key problems described above, which are directly related to the evolution of planets. Original results of studies of the dissipation of the neutral species of planetary atmospheres are considered. The main concepts of planetary aeronomy are introduced, the physical processes that determine rates of energy absorption and atmospheric escape (Section 2) are discussed, and a kinetic Monte Carlo method intended for studying thermal and nonthermal processes of atmosphere dissipation (Section 3) is presented. Data on losses from the atmospheres of Venus and Mars presented in Section 4 are used as an example to critically analyze data from the most recent spacecraft observations in comparison with the results of theory and simulations. Section 5 contains the most recent results of applying the approach presented in the review to studying the rates of atmospheric losses by exoplanets and, more specifically, by hot Jupiters.

2. Basic concepts

2.1 Aeronomic systems of planets, satellites, and comets

Planetary aeronomy problems pertain to many bodies of the Solar System that have gas envelopes, i.e., planets, their satellites, and comets. In most cases, the motion of gas in the envelope is restricted by the gravitational field of the planet or satellite, and such an envelope is referred to as an atmosphere. If the motion of gas in the envelope is not restricted by the attraction of a celestial body, it is referred to as a coma, as is the case with the nucleus of a comet. The presence or absence of a gas envelope is an important indicator that reflects significant features of the origin and evolution of the planet or satellite on a geological time scale. The chemical composition, structure, and dynamics of atmospheres highly depend on the mass and location of the celestial body in the Solar System (to which the initial composition of the atmosphere, thermal and chemical differentiation of the primordial matter, and insolation conditions are related) and on the parameters of orbital and rotational motion. Therefore, even within a small region occupied by terrestrial planets, the properties of their atmospheres are significantly different. The notable differences in the chemical composition of planets and their atmospheres reflect a sequence of evaporation and condensation of the primordial matter in the gas-and-dust accretion disc that formed from the protoplanet nebula, the formation of planets and small bodies, and various stages of their subsequent evolution [19].

2.1.1 Basic length scales and their definition. Relatively dense layers of the lower atmosphere (troposphere) can be treated in the gas dynamic approximation because the mean free path l (the distance between sequential collisions of a particular molecule or an atom) is significantly smaller than the smallest microscopic length scale; the atmospheric pressure height scale is $H = k_B T/(\mu g)$ where T is the kinetic temperature, μ is the average molecular weight, g is the free fall acceleration, and k_B is the Boltzmann constant. The value of H determines the exponential decrease in pressure with growing height. Under appropriate assumptions, the initial kinetic Boltzmann equation can be reduced to this approximation [22]. Because the mean free path increases as the number density decreases, at some altitude in the atmosphere the mean free path becomes approximately equal to the height scale. This altitude is known as the exobase, and the region above the exobase is referred to as the exosphere. more rigorously, the exobase of a planet or satellite with radius R_p is defined as the altitude $h_{exo} = r_{exo} - R_p$ in the atmosphere at which the probability of escape from the atmosphere without subsequent collisions for a molecule (or atom) moving upwards with a velocity exceeding the escape velocity is equal to $\exp(-1)$. The exobase is calculated using the formula

$$P_{exo} = \exp\left(-\int_{h_{exo}}^{\infty} \sigma n(h)\, dh\right) = \exp\left[-\,\mathrm{Kn}^{-1}(h_{exo})\right] = \exp(-1)\,,$$

with the dimensionless parameter $\mathrm{Kn}(h) = \left(\sigma n(h)\, H(h)\right)^{-1}$. Here, $n(h)$ and $T(h)$ are the number density and temperature of gas at an altitude $h = r - R_p$, σ is the elastic scattering cross section, m is the average mass of molecules and atoms, and $g(h) = GM_p/r^2$, where M_p is the mass of the planet and G is the gravitational constant. In the dynamics of rarefied gases, the parameter Kn is referred to as the Knudsen number, which is defined as the ratio of characteristic micro- and macroscopic gas flow scales: $\mathrm{Kn}(h) = l(h)/H(h)$, where the characteristic microscopic scale is the free path length $l(h) = (\sqrt{2}\sigma n(h))^{-1/2}$ and the characteristic altitude-dependent macroscopic scale is the atmospheric height scale $H(h) = k_B T(h)/(mg(h))$. In particular, the condition $\mathrm{Kn} \ll 1$ ensures the correctness of describing the atmosphere in the gas dynamic approximation as a medium in which collisions dominate and which is considered as a continuous medium. At the exobase altitude, $\mathrm{Kn} \sim 1$, and the relation $\sigma n_{exo} H \sim 1$ is often used for determining the exobase. In this estimate, the exobase altitude is attained for the gas concentration along the line of sight $N(r_{exo}) \sim n_{exo} H \sim 1/\sigma$, where r_{exo} is the exobase radius. As the cross section, the value $\sigma \sim (1-3)\times 10^{-15}$ cm^2 is often used, yielding the characteristic value $N(r_{exo}) \sim (1-0.3)\times 10^{15}$ cm^{-2} [22, 23]. On Mercury, the Moon, and many ice bodies in outer regions of the Solar System, the density of gravitationally bound gas along the line of sight is smaller than $1/\sigma$, and hence the escape of atoms and molecules begins directly from the physical surface of the celestial body.

The exobase is typically used as an average altitude h_e from which molecules can escape into open space. However, this approximation is rather rough because the rates of many processes that result in populating the thermosphere with particles having suprathermal energies attain their maximum much lower than the exobase; as a result, the particles with excessive kinetic energy (suprathermal atoms and molecules) can escape from altitudes that are much lower than that nominal level [24]. Stated differently, the structure of the exosphere is determined by the aeronomy of the processes that occur deep in the thermosphere; this requires a description of the transport of particles with an excessive thermal energy. In addition, collisions involving atoms and molecules depend on the energy of the colliding particles, the dominating process usually being so-called forward scattering, whose distribution peaks at small values of scattering angles (an analog of the forward-elongated indicatrix of photon scattering in a gas-and-dust medium); therefore, hard spheres are only a rough approximation of scattering cross sections, and planetary coronas often prove to be populated with molecular species.

2.1.2 Main parameters underlying classifications of atmospheres, comas, and exospheres. The most idealized model is an atmosphere fully bound by gravity, with the velocity of thermal escape exactly equal to zero. Although this model is highly oversimplified, it is convenient for determining the essential composition of the atmosphere. Indeed, in the classic model of atmospheric escape, it is assumed that 1) the atmosphere near and below the exobase is completely determined by collisions and hence the velocity distribution of atoms and molecules is given by the Maxwell function, and 2) directly above the exobase, the collisionless exosphere begins. In this case, the escape outflow due to thermal evaporation of particles from the atmosphere, which has the density $n(r_{exo})$ at the exobase altitude, is described by the classic Jeans formula:

$$F_{esc}(r_{exo}) = \frac{n(r_{exo})\, U}{2\sqrt{\pi}}\,(\lambda + 1)\,\exp(-\lambda)\,,$$

where the dimensionless escape parameter $\lambda = v_{esc}^2/U^2$ is calculated at the exobase altitude h_e. Here, U is the most probable velocity in the Maxwell distribution, $U = (2k_B T/m)^{1/2}$, and the escape velocity at the altitude h_e is defined as $v_{esc}(r_{exo}) = (2GM_p/r_{exo})^{1/2}$. The parameter λ can then be described in physical terms as the ratio of the potential energy of the particle in the gravitational field of the planet to the thermal kinetic energy:

$$\lambda(r_{exo}) = \frac{v_{esc}^2}{U^2} = \frac{GM_p m/r_{exo}}{k_B T} = \frac{r_{exo}}{H}\,.$$

It follows that as $\lambda \to 0$, the atmosphere loses its gravitational bond to the planet and atmospheric outflow occurs in a continuous medium regime owing to the excessive kinetic energy of thermal motion, while in the limit of large values of λ, the atmosphere remains fully gravitationally bound, and the thermal escape is vanishingly small. A comet coma is a characteristic example of the former case, while the latter case is represented best by Jupiter. We note that celestial bodies with small values of λ close to the exobase have the most extended atmospheres.

The limit $\lambda \to 0$ is known as the Jeans limit, which characterizes the maximum possible velocity of thermal escape:

$$\lim_{\lambda \to 0} F_{esc}(r_{exo}) = \frac{n(r_{exo})\,U}{2\sqrt{\pi}} = \frac{1}{4}\,n(r_{exo})\,v_{th}\,,$$

where the thermal velocity is $v_{th} = [8k_B T/(\pi m)]^{1/2} = 1.13U$. Actually, this limit value is equal to the upward thermal flux at the altitude h_e.

To clarify the differences between the atmosphere, coma, and exosphere, we can use an analytic solution of the continuity equation for density and of the momentum equation for an isothermal atmosphere. In this case, the distribution of the number density in the radial direction is described by the formula

$$n(r) = n(r_0)\,\exp\left[\left(\lambda(r) - \lambda(r_0)\right) - \left(M(r) - M(r_0)\right)\right],$$

where $M(r) = (w(r)/U)^2$, and the boundary conditions are set at some conveniently defined altitude. Because the number density $n(r)$ and the radial velocity $w(r)$ are related by the continuity equation, the quantity $4\pi r^2 n(r)\,w(r)$ is constant in the radial direction whenever the chemical composition remains unchanged.

The following limit cases of the above solution are most interesting. In the absence of a radial flow ($M(r) = M(r_0) = 0$), we obtain the condition of hydrostatic equilibrium, under which gravitational attraction is fully balanced by pressure gradient

$$n(r) = n(r_0)\,\exp\left(\lambda(r) - \lambda(r_0)\right) = \lim_{H/r_p \to 0} n(r_0)\,\exp\left(-\frac{r - r_0}{H}\right),$$

where the last passage to the limit is only valid for planets and satellites for which the scale height is small compared to the radius of the celestial body. On the other hand, if the atmospheric flow increases with growing radius, its density decreases when the radius is growing faster than in the hydrostatic approximation. This additional decrease in density is relatively small for a subsonic flow ($M(r) \ll 1$). Bur for larger values of the Mach number M, significant variations of the flow density are observed. As characteristic examples, we mention the solar wind or polar wind in the high-latitude atmosphere of Earth.

2.1.3 Suprathermal particles in planetary atmospheres. In studying the atmospheric gas flow at exosphere altitudes, we should take into account possible losses and the production of atoms and molecules as a result of nonthermal processes such as ion sputtering of neutral gas, ionization and dissociation by electrons, charge exchange with the solar wind, and/or magnetospheric plasma ions.

The category of suprathermal (or 'hot') particles usually includes particles whose kinetic energy is higher than $(5-10)\,k_B T$, where T is the temperature of the background atmospheric gas. The suprathermal particles are produced in various physical and chemical processes, whose products have excessive kinetic energy. If the production rate of such particles populating the range of suprathermal energies is high compared to the rate of their thermalization in elastic collisions, a stable fraction is created that can significantly perturb the locally equilibrium (Maxwell) distribution of the thermal energy of the background atmospheric gas. The list of principal sources of suprathermal particles in the rarefied gas of planetary atmospheres includes:

- charge exchange of high-energy ions of magnetospheric origin in their interaction with neutral species of atmospheric gas;
- dissociative recombination of molecular ions with ionospheric electrons;
- dissociation and dissociative ionization by UV solar radiation and magnetospheric plasma;
- exothermal ion–molecular and neutral chemical reactions;
- sputtering or knock-on of the atmospheric gas by the magnetospheric plasma;
- nonthermal desorption from the surfaces of aerosole and dust fractions.

Photochemical sources, such as dissociative recombination, dissociation under the effect of solar (stellar) photons in the ranges of soft X-ray radiation (soft X-rays, 1–10 nm) and extreme UV radiation (EUV, 10–100 nm), which are usually referred to as XUV photons, and high-energy electrons and exothermal chemical reactions, are characterized by a release of energy of the order of several electron-volts, with a part of this energy possibly stored in the form of internal excitation of reaction products [25]. For example, Fig. 2a shows the calculated function of the distribution of oxygen atoms, which are the main component of the transition region from the thermosphere to exosphere in the upper Martian atmosphere [26]. The thermal distribution function shown a dashed line in Fig. 2a is calculated for an altitude of 230 km for the temperature of the Martian atmosphere $T = 205$ K under the conditions of moderate solar activity. It can be seen that in the range of suprathermal energies, the density of oxygen atoms that are produced owing to a photochemical source (solid curve), namely, dissociative recombination of the molecular oxygen ion, is significantly higher than the density of thermal oxygen atoms (dashed curve) that follows from the Maxwell distribution. A detailed analysis of the contribution of suprathermal oxygen atoms, which is due to the dissociative recombination of the main ionospheric ion, molecular oxygen, to the population of the hot oxygen corona of Mars is presented in Section 4 (see Fig. 5).

Plasma sources include the charge exchange of high-energy ions and sputtering of the atmospheric gas by the

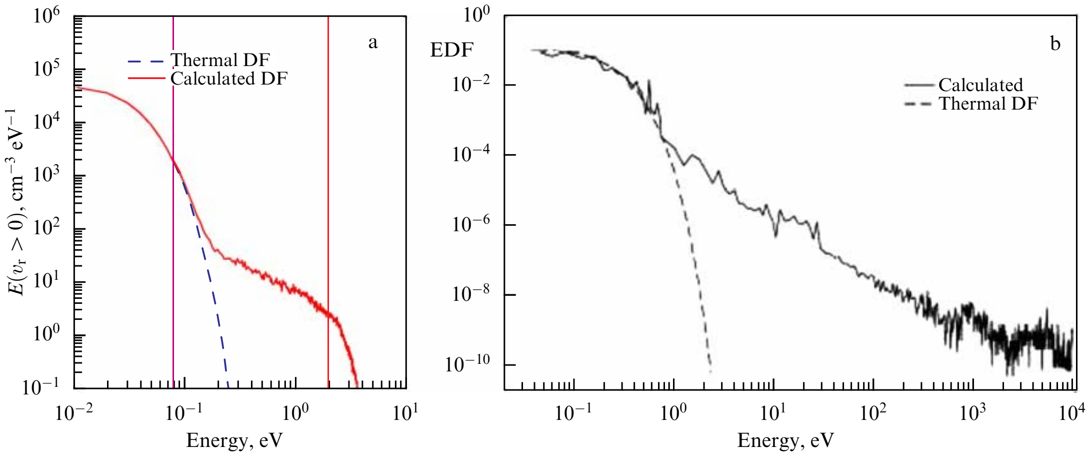

Figure 2. (Color online.) (a) Calculated distribution function (DF) of oxygen atoms at an altitude of 230 km in the upper atmosphere of Mars [26]. The thermal fraction is shown with a dashed curve. The vertical lines indicate conventional boundaries of suprathermal energies and the energy of escape from the atmosphere of Mars. (b) Calculated function of the kinetic-energy distribution (EDF) of oxygen atoms at an altitude of 500 km in the upper atmosphere of Earth [27, 28]. The thermal fraction that corresponds to a temperature of 1170 K is shown with a dashed curve. The range of suprathermal energies $10^{-1}-10^1$ eV is populated with the oxygen atoms produced in photochemical reactions [27], while the range of superthermal energies 10^1-10^4 eV is formed as a result of precipitation of O^+ ions with high kinetic energies [28].

magnetospheric plasma or (in the case of direct interaction) or the plasma of the solar (stellar) wind. Featuring a high efficiency of energy transfer, they produce suprathermal particles with energies up to several hundred electron-volts [3]. As an example, Fig. 2b shows the distribution function, normalized to unity, of oxygen atoms in Earth's upper atmosphere. We can see that the range of suprathermal energies (1–10 eV) is populated with oxygen atoms, products of photochemical reactions [27], while the range of super-thermal energies (10^1–10^4 eV) is formed by the precipitation of oxygen ions O^+ with high kinetic energies [28]. The concentration of suprathermal oxygen atoms is significantly higher than the concentrations of thermal oxygen atoms, which follows from the Maxwell distribution at a temperature of 1170 K in the transition region of Earth's upper atmosphere.

The produced suprathermal particles lose their excessive kinetic energy in elastic and inelastic collisions with the background atmospheric gas. Usually, those processes are considered in a linear approximation under the assumption that the background gas is in thermal equilibrium and only weakly perturbed by suprathermal particles. If the rate of production of suprathermal particles is high, a nonlinear kinetic approximation must be used, because secondary particles with suprathermal energies are also produced. Their subsequent collisions with the background gas result in a cascade production of new suprathermal particles and therefore in significant perturbations of the thermal state of the atmospheric gas. It follows that the kinetics of suprathermal particles can be accurately described using the kinetic Boltzmann equation only on the microscopic level.

2.2 Processes of escape from atmospheres

The planetary atmosphere density decreases as altitude grows; starting with the exosphere altitude particles can run planet-size distances with a very low probability of collisions. At such altitudes, the atoms and molecules whose energy is higher than their gravitational energy and whose radial velocity is directed upward, can escape into open space. At the exobase altitude h_e, a transition occurs from the continuous-medium regime to the rarefied-gas regime, and individual collisions are to be considered using kinetic and/or stochastic methods.

In approximate approaches, such as the Chamberlain model of thermal escape, which is considered in Section 2.3.1, only those atoms that are produced at the level h_e or higher with an energy higher than the escape energy and a velocity directed upward are taken into account. However, for an actual atmosphere, using the exobase altitude alone is ambiguous because the exobase is an extended area that is different for different molecules, and the corresponding models fail to provide the required accuracy. Therefore, the most suitable approach is to use computer simulation of planetary atmosphere dissipation based on kinetic methods, an approach that is currently in wide use [1, 3].

In Section 3, we discuss in detail the kinetic approach to describing the physics and chemistry of the processes that govern production of the neutral planetary corona and atmospheric dissipation. We present the results of simulations for the terrestrial planets that have sufficiently stable atmospheres, wherein atmospheric dissipation is currently a relatively insignificant effect. However, as is shown below, for icy bodies orbiting in the outer areas of the Solar System, the escape of particles from the atmosphere can play a dominant role in their evolution. Those molecules released from the surface of an 'atmosphereless' icy body do leave evidence of the presence of a neutral gas in the gas envelope of such a body, a feature that is especially characteristic of comet atmospheres (comas) at different radial distances from the Sun. In the case of a satellite orbiting a giant planet, this gas can remain gravitationally bound to the planet, forming an almost torus-shaped atmosphere elongated along the satellite orbit. Such atmospheres, which are by their nature an extension of the satellite exosphere, result in partial filling with a neutral gas of the planetary magnetosphere, as is observed for Jupiter's Galilean satellites, Io and Europa.

2.2.1 Thermal escape. We have seen that thermal escape is, by its nature, determined by the temperature at the exobase level, although, formally, the collisional and collisionless regions close to that level cannot be separated by an arbitrary dimensionless boundary. The reason is that the density distribution is a continuous function and therefore the transition from the continuous-medium regime to the regime of free-molecule flow of the atmospheric gas occurs gradually. Furthermore, the number density (and the probability of collisions) at different latitudes and longitudes feature significant variations, such that the local temperature at the level h_e varies in a 3D geometry and the number of particles leaving the atmosphere per unit area and per unit of time follows from the Jeans formula [29, 30]. It should be kept in mind that if the Jeans escape parameter is close to unity and the upper atmosphere deviates from hydrostatic equilibrium, the local velocity distribution of particles is described by the Maxwell distribution with a velocity shift [31, 32], and the probability of particle escape increases as a result of a hydrodynamic outflow (referred to as the planetary wind) [33, 34]. The Jeans and hydrodynamic regimes are the limit cases of thermal escape in which the temperature at the level h_e remains constant or is subject to a strong effect from the atmospheric dissipation regime *itself*.

Results of simulations using the kinetic Monte Carlo method (statistical simulation) show that switching between the hydrodynamic regime and the Jeans regime occurs in a relatively narrow range of escape parameter values [32]. Therefore, it is important to characterize the planetary thermosphere using the assessment of energy balance: in the hydrodynamic regime, the energy balance in the thermosphere sets limitations on the magnitude of atmospheric escape, while in the hydrostatic regime, there is no such dependence. Hydrostatic escape can be considered a limit case of the hydrodynamic regime. An important feature of the hydrodynamic regime is that, essentially, the hydrodynamic escape is limited by the energy available for forming its flow over the entire thermosphere. Stated differently, if the heating rate remains invariable in the thermosphere, then, regardless of the efficiency of the particle outflow at the exobase level, the total escape flow also remains invariable.

2.2.2 Nonthermal escape. A specific feature of nonthermal processes in which the atmosphere loses its particles is that the escape rate does not depend on the temperature at the exobase level. Most of the nonthermal dissipation processes are determined by ions and their behavior in electric and magnetic fields. For example, nonthermal escape that is due to photochemical processes (photochemical escape) is of importance for Mars, but it can hardly be an efficient mechanism for Earth or super-Earths because the maximum kinetic energy the oxygen atom acquires as a result of dissociative recombination of O_2^+ does not exceed several electron-volts, which is lower than the escape energy for a planet more massive than Mars.

Neutral atoms and molecules can be ionized in the planet's atmosphere as a result of photoionization, collisional ionization, and charge exchange with solar-wind ions. If ions are formed around a planet that does not have a magnetic field or whose magnetic field is very weak, they can be accelerated under the effect of the Sun's magnetic field, and some of them can leave the planet. This process of capturing ions is less efficient for a planet such as Earth, because solar or interplanetary electric and magnetic fields are screened at long distances from the planet. In this case, ions can be captured by the planet's magnetosphere. However, different models of hydrodynamic escape from the atmosphere show that the upper atmosphere becomes strongly extended under the effect of strong stellar XUV radiation, with the exobase located at an altitude of several planetary radiuses. If at the same time the strong stellar wind from a young star pushes the magnetopause of the exoplanet's atmosphere down closer than the exobase to the planet's surface, protection by means of its own moderate-strength magnetic field from the effect of the stellar wind plasma on the neutral atmosphere may be inefficient.

If energetic ions are captured by the planet's magnetic field, they can escape from the atmosphere as a result of capturing electrons from slowly moving particles, i.e., charge exchange. Such ions can collide with slow atmospheric particles and, due to momentum transfer, cause the escape of neutral atmospheric particles in the process of atmospheric sputtering or knock off. Because electrons are much lighter than ions, in areas where magnetic-field lines are not closed (magnetic poles or cusps), the atmosphere deviates from strict neutrality. As a result of charge separation between electrons moving upward and ions lagging behind, an additional overall acceleration of ions occurs. Unlike ambipolar diffusion, where the flows of electrons and ions in a weakly ionized plasma virtually coincide, this process results in ions escaping from the atmosphere, giving rise to the so-called polar wind. Updated estimates of the relative importance of thermal and nonthermal mechanisms of atmospheric losses for the terrestrial planets of the Solar System are presented in reviews [3, 35].

We note that nonthermal escape can affect the transition of upper planetary atmospheres from the hydrostatic regime to the hydrodynamic one. It is convenient to relate the flux of the incoming stellar XUV energy and the escape rate from the atmosphere of the planet (exoplanet) to the escape efficiency. For this, a detailed account of contributions from individual processes is required, which would enable not only tracking the energy flows in the chains of atmospheric chemistry reactions but also taking the energy transported within the thermosphere by photo- and secondary electrons into account. All these factors significantly complicate the analysis of the relations between the thermal energy accumulated by the background atmospheric gas and the absorbed energy of solar (stellar) XUV photons, and hence make the calculations of heating efficiency much more difficult [36].

2.3 Approaches to the simulation of the exosphere and atmospheric escape

2.3.1 Chamberlain exobase model. An analytic model for the exosphere gas density that is widely used now was developed by Chamberlain [30]. It is based on the assumptions that the velocity distribution of atmospheric gas molecules at the exobase height h_e is Maxwellian, that collisions can be ignored above the exobase, that the only relevant force is gravity, and that the velocity distribution at altitudes $h > h_e$ is obtained from the Liouville equation. Three populations of particles were considered that depend on the trajectory type: ballistic, satellite, and escaping. Using the Liouville equation, an analytic formula was derived for the density of each population at altitudes larger than h_e. This approach was generalized to a nonuniform exobase [37] and a rotating planet [38, 39]. Velocity distributions produced by photo dissociation and atmospheric sputtering have also been used. For instance, it was shown that in order to fit the recent INMS (Ion and Neutral Mass Spectrometer) Cassini spacecraft measurement of the exospheric density of Titan, a satellite of Saturn, it is necessary to take the population of high-energy tails of the distribution function into account and, in this way, to represent the suprathermal (hot) particles produced at altitudes below the exobase [40]. The full distribution function can be described in this case by a kappa distribution or a Maxwellian function combined with a power-law distribution for the high-energy tail. A best fit was found for the atmospheric corona gas densities in a narrow range of altitudes using a kappa distribution to account for both suprathermal and thermal species of the atmospheric particle fractions.

Coronas like Titan's exosphere proved to be populated with nonthermal species, requiring a description of suprathermal-energy particle production below the exobase, where collisions cannot be disregarded. Accordingly, deviations from local thermal equilibrium (LTE) start at $\mathrm{Kn} \sim 0.1$, which occurs at 650 km in Titan's atmosphere. Therefore, production and transport of suprathermal particles in the planetary corona requires solving the Boltzmann equation or performing Monte Carlo simulations [41].

2.3.2 Kinetic Boltzmann equation for suprathermal particle transport. In the so-called two-stream approximation, the flux of suprathermal (hot) particles in a background thermal atmosphere is derived from the full Boltzmann transport equation (see, e.g., [42]). Separating the flux into upward $\Phi^+(E, h)$ and downward $\Phi^-(E, h)$ components, where E is the kinetic energy and h the altitude, results in coupled linear equations that are solved for a range of altitudes up to h_e. The velocity distribution for the suprathermal particles at the exobase is $f(h, v) = (\Phi^+(E, h) + \Phi^-(E, h))/v(E)$, where $v(E)$ is the speed corresponding to the kinetic energy E [43]. The exospheric structure and escape rate are then determined using the Liouville equation. Studies [44–46] modeled the first detection of the suprathermal fraction of O atoms in Venus's exosphere produced by dissociative recombination of the O_2^+ molecular ion. The measured branching ratios for dissociative recombination and the vibrational distribution of the ground state of the O_2^+ ion were also used for modeling Mars's upper atmosphere for solar minimum and maximum conditions on Mars [47]. The role of CO^+ dissociative recombination and photodissociation of the CO molecules in Mars's aeronomy was calculated similarly [48].

Approaches have been developed to solve a linearized Boltzmann equation that describes the atmospheric gas flow in the transition region (see, e.g., [2, 49, 50]). This approximation is used to describe the flow of suprathermal or minor species through the background atmosphere, assuming that their effect on the thermal state is negligible. In [51], the Boltzmann collisional term is calculated for endothermic and/or exothermic reactions between species that both have Maxwellian distributions and scatter isotropically. The results were successfully compared with the Monte Carlo test particle simulations described below. The results include the distributions of suprathermal O in the Venusian and Martian atmospheres produced by dissociative recombination of O_2^+, including collisions with thermal atmospheric oxygen atoms.

2.3.3 Kinetic Monte Carlo simulation. The Direct Simulation Monte Carlo (DSMC) method, a stochastic method used to describe a rarefied gas, is equivalent to solving the Boltzmann equation. It treats both the dynamic and stochastic nature of the gas at the molecular level [52]. The method is valid if the collisions are statistically independent, multiparticle collisions are negligible, and the collision time is small compared to the time between collisions. All types of collisions can be accounted for, including those between atmospheric particles, and nonlinear processes can thus be included [26–28, 53–56]. Each species is described in terms of its phase-space distribution. The motions of representative particles, each assigned a weight, are followed taking collisions and forces into account. Source distributions and collisions are typically treated using Monte Carlo algorithms. The DSMC method is resource consuming when the domain in the atmospheric gas flow under study is highly collisional, but is useful for describing the transition from the collisional to collisionless regime [1, 57]. It has been successfully used to simulate heating of the exobase region and studying the coronal structure and escape using knowledge of the processes that produce suprathermal atoms and molecules. DSMC simulations have been applied to the exobase region of Mars [26, 56, 58, 59], Titan [24, 60], and Jupiter's satellite Europa [55, 61], as well as to a comet's coma [1, 62, 63] and the upper atmosphere of exoplanets [64].

3. Kinetic Monte Carlo method for studying the dissipation of planetary atmospheres

3.1 Kinetics of suprathermal particles

We now consider in more detail the kinetic Monte Carlo method (stochastic simulation method based on the set of Boltzmann equations) and its applications to thermal and nonthermal dissipation of particles from a planetary atmosphere on the basis of discrete mathematical models.

Let a rarefied gas in the planetary atmosphere consist of α_i, $i = 1, \ldots, S$, atoms and molecules in a physical volume V. Each particle of a species α_i (atom, molecule, and/or their ion) is characterized by the mass m_i, location $\mathbf{r}_i \in V$, velocity $\mathbf{c}_i$, and a set of quantum numbers $\mathbf{z}_i$ for each possible level of internal excitation. These chemically different species interact through collisions via $m = 1, \ldots, M > 1$ chemical reactions specified by the dynamic schemes

$$m : \alpha_i(\mathbf{c}_i, \mathbf{z}_i) + \alpha_j(\mathbf{c}_j, \mathbf{z}_j) \rightarrow \alpha_k(\mathbf{c}'_k, \mathbf{z}_k) + \alpha_l(\mathbf{c}'_l, \mathbf{z}_l) . \qquad (1)$$

To provide a general description, we treat reactions (1) as a dynamic process that involves both elastic ($\alpha_i = \alpha_k$ and $\alpha_j = \alpha_l$) and inelastic ($\alpha_i = \alpha_k$ and $\alpha_j = \alpha_l$) collisions (however, internal excitation levels are different: $\mathbf{z}_i \neq \mathbf{z}_k$ and/or $\mathbf{z}_j \neq \mathbf{z}_l$), as well as chemical reactive collisions ($\alpha_i \neq \alpha_l$ and/or $\alpha_j \neq \alpha_l$).

The probabilities of reactions (1) are determined using scattering functions

$$g_{ij}\, \mathrm{d}\sigma_m = |\mathbf{c}_i - \mathbf{c}_j|\, \sigma_m\big(|\mathbf{c}_i - \mathbf{c}_j|, \Omega\big)\, \mathrm{d}\Omega ,$$

where $\mathrm{d}\sigma_m$ is the differential scattering cross section for reaction (1), $g_{ij} = |\mathbf{c}_i - \mathbf{c}_j|$ is the relative velocity, and Ω is the solid scattering angle. Each channel in reaction (1) is specified by the corresponding elastic σ_m^{el}, inelastic σ_m^{in}, or chemical reactive σ_m^{r} cross section, such that

$$\sigma_m = \sigma_m^{\mathrm{el}} + \sigma_m^{\mathrm{in}} + \sigma_m^{\mathrm{r}} .$$

The scattering functions that depend on the potential of interaction between reacting particles are usually calculated using quantum mechanical methods or measured in laboratory experiments. The velocities of the particles produced in reaction m are determined using the mass, momentum, and total energy conservation laws for interacting molecules, while their directions are selected in accordance with the probabilistic scattering function

$$\frac{\sigma_m\big(|\mathbf{c}_i - \mathbf{c}_j|, \Omega\big)}{\int \sigma_m \, \mathrm{d}\Omega} \, .$$

The evolution of a chemically reacting system on a microscopic-description level follows from the solution of the set of Boltzmann kinetic equations

$$\frac{\partial F_{\alpha_i}}{\partial t} + \mathbf{r}\,\frac{\partial F_{\alpha_i}}{\partial \mathbf{r}} + \frac{\mathbf{G}}{m_{\alpha_i}}\,\frac{\partial F_{\alpha_i}}{\partial \mathbf{c}} = Q_{\alpha_i} + \sum_m J_m^{\alpha_i}(F_{\alpha_i}, F_{\alpha_j}) \, , \qquad (2)$$

with initial and boundary conditions for the atmospheric gas in a volume V subject to the effect of the planet's external field $\mathbf{G}$ and under physical assumptions such as the rarefied state of the gas or rapidly decreasing particle interaction ranges in collisions [1, 65, 66]. The gas state is described on a microscopic level using distribution functions of gas particles by velocity and internal state excitation $F_{\alpha_i}(t, \mathbf{r}, \mathbf{c}) = n_{\alpha_i}(t, \mathbf{r}, \mathbf{z})\, f_{\alpha_i}(t, \mathbf{r}, \mathbf{c})$, where $n_{\alpha_i}(t, \mathbf{r}, \mathbf{z})$ is the number density of a particle in a state $\mathbf{z}$ and $f_{\alpha_i}(t, \mathbf{r}, \mathbf{c})$ is a single-particle velocity distribution function normalized to unity. Source functions $Q_{\alpha_i}(t, \mathbf{r}, \mathbf{c})$ determine the rates of production of suprathermal particles in photochemical and/or plasma processes. The collision integral $J_m^{\alpha_i}(F_{\alpha_i}, F_{\alpha_j})$ in the right-hand side of the kinetic equations describes how the gas state changes as a result of chemical reactions:

$$J_m^{\alpha_i}(F_{\alpha_i}, F_{\alpha_j}) = \int g_{ij}\, \mathrm{d}\sigma_m\, \mathrm{d}\mathbf{c}_j \big[e_m F_{\alpha_k}(\mathbf{c}'_k)\, F_{\alpha_l}(\mathbf{c}'_l) - F_{\alpha_i}(\mathbf{c}_i)\, F_{\alpha_j}(\mathbf{c}_j)\big] \, , \qquad (3)$$

where e_m is the normalization factor of phase volume conservation in chemical reactions.

The kinetics of a rarefied atmospheric gas on the microscopic level is fully determined by the dynamic and probabilistic characteristics of molecular collisions, the scattering functions, and the distribution functions of colliding particles by translational and internal degrees of freedom. Accordingly, the chemical evolution of the atmospheric gas has an involved structure of the kinetic rates of exchange by translational and internal energies.

The kinetics and transport of suprathermal particles in planetary coronas are apparently nonequilibrium, because both the production and transport of suprathermal particles from the underlying atmospheric layers and nonthermal losses result together in deviations of the atmospheric gas state from LTE. The gas flow in the planetary corona is then adequately described either as a mixed kinetic system if perturbations in the thermal state of the background atmospheric gas caused by suprathermal particles are small, or by a fully kinetic set of Boltzmann equations (2) if those perturbations are significant and the planetary corona becomes hot.

In the kinetic theory of rarefied gases and its applications to aeronomy problems, a number of methods have been developed for studying the gas dynamics and kinetics in conditions close to LTE [22, 67]. An analysis of strongly nonequilibrium systems ($\varepsilon_\alpha \sim 1$) is very involved due to the mathematical complexity of the Boltzmann kinetic equations (nonlinear and multiple integrals), which requires developing new approaches.

3.2 Numerical kinetic model for studying atmospheric escape flows

An approach that seems to be quite promising is to develop object-oriented discrete mathematical models that use a probabilistic interpretation of collisions in an ensemble of model particles. This class includes the DSMC method [52] and its modification for studying nonequilibrium processes in chemically active gases [68, 69] for the chemistry of planetary atmospheres [1, 70–72] and astrochemistry [73, 74]. The main idea of this approach to solving the system of Boltzmann equations (2) is to approximate measures $F_\alpha(t, \mathbf{r}, \mathbf{c})\, \mathrm{d}\mathbf{r}\, \mathrm{d}\mathbf{c}$ with a discrete numerical model with point-like measures, a system or ensemble of model particles.

Below is a general scheme for developing a numerical discrete model intended for studying the production, kinetics, and transport of suprathermal particles in a planetary corona:

• the scales, local average free path time and length for atmospheric gas particles are to be taken as characteristic time and space scales because the numerical model corresponds to a microscopic (molecular) level of the description of the gas state in planetary corona;

• atmospheric gas parameters deviate greatly in the transition region (hot planetary corona) from those that are specific to gas flow and determined by collisions in a relatively dense thermosphere and those that are specific to free molecular (virtually collisionless) flow in the exosphere, i.e., the gas flow in the planetary corona has significant density and temperature gradients;

• usually, significant differences are observed between the concentrations of suprathermal particles that are produced in photochemistry and sputtering by the magnetosphere plasma and the background atmospheric gas.

To take those characteristic features of the formation of hot planetary coronas into account in developing a numerical model, the following approaches are to be used:

— split the solution of the initial kinetic system (2), according to physical processes, into the stages of simulation of suprathermal particle sources, collisional relaxation of those particles in physical and chemical reactions, and collisionless transport of suprathermal particles under the effect of the planet's gravitational and magnetic fields on a discrete time scale;

— stochastically simulate production of suprathermal particles and their local physical and chemical kinetics using analog weighted Monte Carlo algorithms;

— calculate trajectories of suprathermal particles using finite-difference algorithms disregarding collisions in the planetary corona.

Similarly to the method of splitting by physical processes, we use the following discrete presentation of time:

$$t_p = p\Delta t \, , \quad p = 0, 1, \ldots, \Delta t > 0 \, , \qquad (4)$$

where the time step Δt corresponds to the minimum average time of the free path of molecules, which is typically calculated using parameters of suprathermal particles and the atmospheric gas near the lower boundary of the planetary corona, where the atmospheric gas is well mixed owing to collisions. Such a step Δt, which is usually small, enables us to treat the local kinetics and free transport of suprathermal particles separately.

The region where the hot corona is formed, the transition region between a dense thermosphere and a strongly rarefied exosphere, is divided into a finite set of nonoverlapping cells,

$$\mathrm{G} = \bigcup_{h=1}^{H} \mathrm{G}_h\,, \tag{5}$$

and the characteristic size of the cells is taken to be less than (or the same as) the local free path.

Next, we assume that each model particle is characterized by the vector

$$\mathbf{x}_i = (\mathbf{r}_i, \mathbf{c}_i, w_i)\,, \tag{6}$$

where a species α particle has the geometrical coordinates $\mathbf{r}_i$, velocity $\mathbf{c}_i$, and statistical weight w_i, i.e., the vector $\mathbf{x}_i$ is a discrete measure that corresponds to the distribution function $F_{\alpha_i}(t, \mathbf{r}, \mathbf{c}) = n_{\alpha_i}(t, \mathbf{r}, \mathbf{z}) f_{\alpha_i}(t, \mathbf{r}, \mathbf{c})$. We note that the idea of statistical weight is that it is proportional to the number of actual molecules represented by the specific model particle. Following the main concept of the stochastic approach, to describe the construction of a discrete kinetic model, we introduce two families of model particles in each cell (5):

$$\begin{cases} \mathbf{X}^{(1)}(t) = \bigcup\limits_{\alpha=1}^{S} \bigcup\limits_{i=1}^{N_\alpha} \mathbf{x}_i^{(1)}(t)\,, \\ \{\mathbf{x}_i^{(1)}(t)\,, \quad i = 1, \ldots, N_\alpha^{(1)}(h)\,, \quad h = 1, \ldots, H\}\,, \end{cases} \tag{7}$$

$$\begin{cases} \mathbf{X}^{(2)}(t) = \bigcup\limits_{\alpha=1}^{S} \bigcup\limits_{i=1}^{N_\alpha} \mathbf{x}_i^{(2)}(t)\,, \\ \{\mathbf{x}_i^{(2)}(t)\,, \quad i = 1, \ldots, N_\alpha^{(2)}(h)\,, \quad h = 1, \ldots, H\}\,, \end{cases} \tag{8}$$

where $t \in [t_p, t_{p+1}]$ and N_α is the number of species α model particles in a cell h. Here, superscript (1) corresponds to the step of simulation of free particle transport in region G, and superscript (2) to the step of simulation of the local kinetics of production and collisional relaxation of suprathermal particles in each cell during the time interval $[t_p, t_{p+1}]$.

The evolution of particle system (7) (the stage of free molecular transport) in the entire region G under investigation is defined as follows. The initial state of the system is the initial distribution if $p = 0$ and, if $p > 0$, the state of system (8) for t_p, i.e., $\mathbf{X}^{(1)}(t_p) = \mathbf{X}^{(2)}(t_p)$. Then the evolution of numerical system (7) is determined by the equations

$$\begin{cases} \dfrac{\mathrm{d}\mathbf{r}_i^{(1)}(t)}{\mathrm{d}t} = \mathbf{c}_i^{(1)}(t)\,, \\ \dfrac{\mathrm{d}\mathbf{c}_i^{(1)}(t)}{\mathrm{d}t} = \dfrac{\mathbf{G}}{m_\alpha}\,, \\ w_i^{(1)}(t) = w_i^{(1)}(t_p)\,. \end{cases} \tag{9}$$

The velocities of model particles change under the effect of external fields, while the statistical weights of the particles at the free-transport stage do not change. Equations (9) yield a solution of the Boltzmann equations without sources and collisions for the time interval $[t_p, t_{p+1}]$.

The evolution of particle system (8) (the stage of the local kinetics of production and collisional relaxation of suprathermal particles) in each cell (5) is determined as follows. The initial state of system (8) is the final state of system (7) at t_{p+1}, i.e., $\mathbf{X}^{(2)}(t_p) = \mathbf{X}^{(1)}(t_{p+1})$. The gas is considered to be uniform within the cell and, accordingly, the locations of particles do not change. This stage is divided into two steps: first, in accordance with the functions of photochemical or plasma sources, suprathermal particles are produced in each cell, and then the stochastic simulation method is used to randomly draw collisions of model suprathermal particles with background-gas particles in the time interval $[t_p, t_{p+1}]$. At the first step, in accordance with the source functions $Q_{\alpha_i}(t, \mathbf{r}, \mathbf{c})$, a specified number of new model particles, for example $N_\alpha^{(q)}$, is produced in numerical system (8):

$$\begin{cases} \mathbf{X}^{(2)^{\min}_{\text{new}}}(t_p) = \mathbf{X}^{(2)}(t_p) \bigcup \mathbf{X}^{(q)}(t_p)\,, \\ \mathbf{X}^{(q)}(t_p) = \bigcup\limits_{\alpha=1}^{S} \bigcup\limits_{i=N_\alpha}^{N_\alpha + N_\alpha^{(q)}} \mathbf{x}_i^{(q)}(t_p)\,, \end{cases} \tag{10}$$

where, in the state vectors $\mathbf{x}_i^{(q)}(t_p)$ of new model particles, geometric coordinates are selected at random, velocities $\mathbf{c}_i^{(q)}(t_p)$ are selected in accordance with the energy spectra of source functions, and the statistical weights of the particles are determined as

$$w_i^{(q)}(t_p) = \frac{\Delta t}{N_\alpha^{(q)}} \int \mathrm{d}\mathbf{c}_i\, Q_{\alpha_i}(t, \mathbf{c}_i)\,.$$

A detailed description of the probabilistic algorithms for choosing collision statistics at the second step of calculating collisional relaxation is presented in Section 3.3. Here, we only note the main idea of randomly selecting the specific collision (reaction m) that follows from the methodology for using the weighted Monte Carlo scheme for analyzing multicomponent systems with significantly different concentrations [1, 52, 75, 76].

For example, let the ith and jth reacting particles be selected with statistical weights $w_i^{\alpha_i}$ and $w_j^{\alpha_j}$. Then the velocities of the particles produced in this reaction can be found from the mass, momentum, and energy conservation laws. As a result of the reaction, we take production of the following particles:

$$\left[\{\mathbf{r}_i, \mathbf{c}_i, w_i^{\alpha_i} - W\}, \{\mathbf{r}_j, \mathbf{c}_j, w_j^{\alpha_j} - W\}, \{\mathbf{r}_k, \mathbf{c}_k', W\}, \{\mathbf{r}_l, \mathbf{c}_l', W\}\right],$$

where W is a weight transfer function that depends on the state of the numerical model and parameters of the reacting particles. Therefore, this implementation of reaction m corresponds to transferring the weight W, which is equal to (or less than) the minimum weight of one of the reacting particles, between the actual number of atmospheric-gas molecules and suprathermal particles. Schemes with statistical drawings of collisions with weight transfer are rather efficient in simulating the kinetics of suprathermal particles where significant differences between concentrations of suprathermal particles and background atmospheric gas can occur.

3.3 Stochastic kinetic equation for suprathermal particles

The stage of simulating the kinetics of production and collisional relaxation of suprathermal particles in each partition cell (5) is the most complicated one. In this section, we present a detailed description of the procedure for stochastic simulation of the chemical kinetics of suprathermal particles in a specific cell (and we omit the indices denoting the geometric location of model particles).

The probabilistic description of the chemical kinetics of a rarefied atmospheric gas is based on the theory of random processes [77, 78]. Based on the fundamental definitions of that theory, the evolution of a chemically reacting atmospheric gas is described by the kinetic equation [1, 65, 66, 70]

$$\frac{\partial}{\partial t}\,\varphi(\mathbf{X}, t) = V^{-1} \sum_m \sum_{i,j} \int g_{ij}\, \mathrm{d}\sigma_m \big[e_m \varphi(\mathbf{X}_{ij}^m, t) - \varphi(\mathbf{X}, t) \big]\,. \tag{11}$$

Equation (11), which is linear in the distribution $\varphi(\mathbf{X}, t)$ of the probability density of a state $\mathbf{X}$ of the gas at an instant t, is called the stochastic (or master) kinetic equation of the chemical kinetics of a rarefied gas in the stochastic approximation. In the case of elastic binary collisions, Eqn (11) reduces to the well-known Prigogine–Kac equation for the N-particle velocity distribution function [78, 79].

Stochastic kinetic equation (11) describes the evolution of a uniform Markov jump process in accordance with the definitions given below.

State of the gas. In the stochastic approximation, the concentrations and velocities of suprathermal and thermal species of the rarefied gas in a specified physical volume V are treated as random variables. Accordingly, the rarefied gas is represented as a system of a finite number of particles $N = N_1 + \ldots + N_\alpha + \ldots + N_S$; for each particle belonging to a subset $(1, \ldots, i, \ldots, N_\alpha)$ that corresponds to the α-species of the gas, a vector $\mathbf{x}_i^{\alpha_i} = (\mathbf{c}_i, w_i^{\alpha_i})$ is defined that contains the velocity and statistical weight of that particle. The state of the numerical model is then described as

$$\mathbf{X} = \bigcup_{\alpha=1}^{S} \mathbf{X}^\alpha = \bigcup_{\alpha=1}^{S} \bigcup_{i=1}^{N^\alpha} \mathbf{x}_i^\alpha\,, \tag{12}$$

i.e., as a set of discrete measures that approximate the corresponding distribution function $F_\alpha(t, \mathbf{c}) = n_\alpha(t, \mathbf{z}) f_\alpha(t, \mathbf{c})$.

Jump transitions $\mathbf{X} \to \mathbf{X}'$ *between states of the numerical system* are presented as instantaneous changes in particle characteristics in accordance with the dynamic schemes of chemical reactions. We let the next transition correspond to implementation of reaction m, and the model reacting particles α_i and α_j be selected; then

$$\mathbf{X} \to \mathbf{X}' = \mathbf{X}_{ij}^m\,, \tag{13}$$

where the state of the model after the selected transition is

$$\mathbf{X}_{ij}^m = \begin{cases} \mathbf{X}^{\alpha'}, \quad \alpha' \neq \alpha_i, \alpha_j, \alpha_k, \alpha_l\,, \\ {}^{(-)}\mathbf{X}_i^{\alpha_i} = \big\{ \ldots, (\mathbf{c}_i, w_i^{\alpha_i} - W_{ij}^m), \ldots \big\}\,, \\ {}^{(-)}\mathbf{X}_j^{\alpha_j} = \big\{ \ldots, (\mathbf{c}_j, w_j^{\alpha_j} - W_{ij}^m), \ldots \big\}\,, \\ {}^{(+)}\mathbf{X}^{\alpha_k} = \mathbf{X}^{\alpha_k} \bigcup (\mathbf{c}_k', W_{ij}^m)\,, \\ {}^{(+)}\mathbf{X}^{\alpha_l} = \mathbf{X}^{\alpha_l} \bigcup (\mathbf{c}_l', W_{ij}^m)\,. \end{cases} \tag{14}$$

Here, W_{ij}^m is the transfer function in reaction m defined such that the statistical weights of the particles are nonnegative, i.e.,

$$W_{ij}^m \leqslant \min(w_i^{\alpha_i}, w_j^{\alpha_j})\,.$$

The velocities of the particles after the reaction are found from conservation laws, and their directions are statistically determined by differential cross sections.

Probabilities $\omega(\mathbf{X} \to \mathbf{X}')$ *of transitions* are discrete representations of the kinetic rates of chemical reactions,

$$\omega(\mathbf{X} \to \mathbf{X}') = \omega_{ij}^m = V^{-1} g_{ij} \sigma_m(g_{ij})\,. \tag{15}$$

The total rate of transitions is only determined by the state of the model as a whole:

$$\omega(\mathbf{X}) = \sum_m \sum_{i,j} \omega_{ij}^m\,. \tag{16}$$

The probabilistic distribution of time $\tau(\mathbf{X} \to \mathbf{X}')$ *between sequential transitions* is described by the exponential law:

$$P\big\{\tau(\mathbf{X} \to \mathbf{X}') \leqslant \tau\big\} = 1 - \exp\big(-\omega(\mathbf{X})\,\tau\big)\,, \tag{17}$$

because $\mathbf{X}(t)$ is a Markov jump process.

Equations (12)–(17) provide a rigorous definition of a random process $\mathbf{X}(t)$ that describes the chemical kinetics of a rarefied gas in the stochastic approximation. The linearity of the stochastic kinetic equations is an important advantage of the kinetic approach, which enables efficient schemes for simulating Eqn (11) to be developed using the Monte Carlo method [1, 65, 66, 70].

3.4 Analog Monte Carlo algorithm for solving the stochastic kinetic equation

Direct methods for solving the master (stochastic or chemical) kinetic equation consist in developing and numerically implementing a set of equations for the probabilities of all possible trajectories of the state of a chemically reacting rarefied gas. Unfortunately, this direct procedure can only be implemented for a number of very simple chemical systems [73, 74, 80] while for real systems of chemical reactions it encounters substantial computational difficulties.

The Monte Carlo method that generates a sampling of individual state trajectories of a chemically reacting gas is an efficient tool for studying complex chemical systems in the stochastic approximation and somewhat reducing those difficulties. The procedure that generates a single trajectory is much simpler: a sequence of transitions between the states of the chemically reacting gas is to be decided at random based on suitable distributions of probabilities. To implement this procedure, a uniform Markovian jump-like chain $\mathbf{X}(t)$ is replaced with an equivalent uniform Markov chain ${}^{(s_t)}\mathbf{X}$, where s_t is the number of transitions (13) between states (12) during time t. This equivalent correspondence is a basis of the algorithmic implementation, because the procedure of numerical implementation of the chain ${}^{(s_t)}\mathbf{X}$ is rigorously defined by Eqns (12)–(17). The described procedure is an analog algorithm of the Monte Carlo method for solving stochastic kinetic equation (11).

The rigorous playout scheme for the Markov chain ${}^{(s_t)}\mathbf{X}$ on discrete time mesh (4) includes, in accordance with Eqns (12)–(17), the following operations at a time step Δt starting with the state ${}^{(0)}\mathbf{X} = \mathbf{X}(t_{p-1})$ at the instant t_{p-1}:

— the next transition s is selected. Transition rate (16) is calculated and the waiting time $\tau^{(s)}$ for this transition is randomly determined from probabilistic distribution (17). This time is input into the transition counter: $T^{(s)} = T^{(s-1)} + \tau^{(s)}$;

— if the transition counter satisfies the condition $T^{(s-1)} \leqslant t < T^{(s)}$, the new state $\mathbf{X}(t_p) = {}^{(s-1)}\mathbf{X}$ is adopted. Otherwise, the next transition is selected in accordance with probabilities (15), (16), the new state of the model is calculated, and all operations are repeated beginning from the previous step.

These algorithmic steps form an exact analog Monte Carlo method for solving the stochastic kinetic equation for

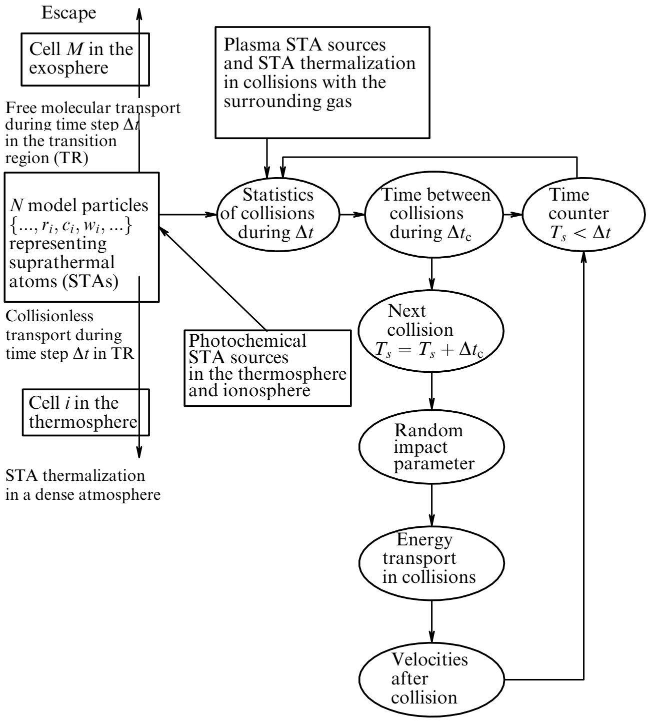

Figure 3. Diagram of the numerical implementation of the analog Monte Carlo algorithm for solving the stochastic kinetic equation [24].

a chemically reacting gas [65, 70, 72]. However, in practice, in modeling the kinetics of suprathermal particles, approximations of this conceptual algorithm are frequently used (Fig. 3). Such approximations take the above-mentioned specific features of the kinetic system under consideration into account, namely:

• in selecting the next transition, an efficient approximation of the highest (majorant) rate [81] is made, with the probability of collision of a selected pair estimated using the maximum possible rate (15),

$$\omega_{ij}^{m,*} = V^{-1} g_{ij} \sigma_m(g_{ij}) \max\left(w_i^{\alpha_i}, w_j^{\alpha_j}\right),$$

and the probabilities $\zeta_{ij}^{m} = \omega_{ij}^{m,*} / \max\left(\omega_{ij}^{m,*}\right)$ enable selecting in the most efficient way the sequence of collisions in the model;

• for the selected transition s, the multichannel character of the played-out performed reaction m is taken into account, i.e., this transition is considered to be a simultaneous playout all possible channels: elastic, inelastic, and chemical reactive. For each of these channels, the corresponding weight $W_{ij}^{m} \sigma_m^{(..)} / \sigma_m$ is transferred, in proportion to the partial cross section for the given channel and the total cross section of the reaction;

• because the algorithmic steps of 'adding' suprathermal particles in accordance with the source functions and the playout of collisional processes (13) involve the production of new model particles, the total number of model particles in the numerical model is to be controlled. An efficient means is here the so-called clusterization of model particles [82], in which groups of model particles with similar characteristics are combined into a single particle with weighted parameters, which allows controlling the total number of model particles.

Owing to the linearity of Eqn (11) and hence of the analog Monte Carlo algorithm that implements that equation, physical and chemical characteristics of the gas are calculated by averaging trajectories of the random process $\mathbf{X}(t)$.

4. Dissipation of the atmospheres of Venus and Mars

The atmospheres of Venus and Mars consist primarily of CO_2 with minor admixtures of Ar, O_2, O, N_2, and CO and a number of other species. In the exosphere, hydrogen and oxygen atoms dominate, with a minor admixture of helium and carbon atoms, while the main component of the ionosphere is the molecular ion O_2^+, which is produced as a result of the rapid reaction with the neutral atom O of the main photoionization product, the CO_2^+ ion. The peak of the O_2^+ density in the Martian ionosphere is reached at altitudes where the optical thickness, as a result of absorption of hard solar UV radiation by CO_2 molecules, is unity ($\sim$ 120–130 km in the subsolar point). The O_2^+ ions dissociatively recombine with thermal electrons, producing suprathermal O atoms that populate the exosphere. Although the collisional domains of the upper atmospheres of Mars and Venus (below $\sim$ 200 km) are not subject to the direct effect of solar wind, the uppermost atmospheric layers are not protected from the effect of solar plasma by the planetary magnetic field, as is the case with Earth and the giant planets. At the same time, the extended ionosphere forms a conducting obstacle to solar wind plasma on the dayside. Here, the solar wind is slowed down, its speed diminishes from supersonic to subsonic, a shock wave is created, and a magnetic layer is formed in the turbulent plasma that appears behind the shock wave.

A weak magnetic field and its nonuniform distribution give rise to specific features of the interaction of solar wind with the Martian atmosphere that cause the formation of an irregular quasi-magnetosphere of the planet. The interplanetary magnetic field (IMF) moving with the solar wind induces currents in the upper layers of the ionosphere, in accordance with Faraday's law. Those currents generate magnetic fields that are close to tangent to the surface, thus shaping the overall configuration of the magnetic field, which is compressed and arranged in folds within the magnetic layer, and making the plasma flow around the planet. The induced quasi-magnetosphere of Mars is created behind the planet; parts of its magnetic tail are stretched in opposite directions. Very similar topology is discovered on Venus, which has no magnetic field whatsoever but has a dense atmosphere. However, Mars, unlike Venus, has spatially nonuniform paleomagnetic fields (with the maximum residual strength reached at about one third of the southern hemisphere of the planet's crust, between 120° and 240° eastern longitude), which, rotating with the planet, affect the global character of Mars's interaction with the solar wind at distances up to 1,000 km. In turn, the topology of those fields results in a nonuniform structure of precipitation of electrons, in particular, on the night side, where the ionosphere that is being formed has a 'patchy' and rather nonuniform structure.

Mars and Venus are surrounded by a uniquely diversified electrodynamic environment in which atmospheric escape occurs. Interaction between solar wind structures (sectorial boundaries, corotation interaction regions, coronal gas outbursts, beam instabilities, etc.) induced by the quasi-magnetosphere and rotating fields and precipitation into this environment of energetic particles, as well as variability of the flux of hard solar UV radiation, result in a broad range of interrelated plasma processes that have a significant impact on atmospheric escape.

The processes of escape from the Martian and Venusian atmospheres are naturally divided into two main categories depending on the charge of the specific atom or molecule at the time it attains the escape energy on a trajectory that does not cross collisional regions of the atmosphere. These categories are the escape of neutral particles and of ions. However, these categories are not fully separated: a neutral particle with an energy sufficient for escape can be ionized and detected by spacecraft instruments as an escaping ion.

In this section, we discuss dissipation of neutral components in the upper atmospheres of Mars and Venus. For example, the neutral particles that populate the atmosphere of Mars (atomic hydrogen, oxygen, nitrogen, argon, and carbon) are transported to the exosphere from the thermosphere as a result of the following thermal and nonthermal processes: thermal (Jeans) evaporation, photochemical reactions, and sputtering caused by ions with high kinetic energies. These processes are the three main ways by which the primary population of the atmosphere is established. The quantitative analysis of the velocities of the suprathermal-energy particles enables determining whether they are gravitationally bound to the planet, i.e., whether they are able to escape from the atmosphere.

Although the exobase altitude h_e is not a strictly defined boundary and significant escape can occur from a transition region whose size is several times the height H of the uniform atmosphere below the exobase [25, 26], the exobase nevertheless remains a convenient altitude where transition from the collisional state of the gas in the upper atmosphere to the collisionless regime occurs. The exobase altitude on Mars, which is close to 200 km, varies depending on the Martian season of the year and the solar activity cycle [56, 59]. The escape velocity at an altitude of 200 km is 4.87 km s^{-1}, with the equivalent kinetic energy 0.124 eV per proton mass. A neutral atom or molecule can gain the kinetic energy sufficient to leave the atmosphere in a number of ways (Fig. 4). First, it can be the thermal particles populating the tail of suprathermal energies in the Maxwell distribution above the local escape energy, a phenomenon that corresponds to the Jeans escape process. Second, an atom or a molecule having an energy sufficient for escape can be produced in an exothermic reaction in atmospheric photochemical processes, a phenomenon that corresponds to photochemical escape. Finally, ions or neutral particles having high kinetic energy that precipitate into the atmosphere can transfer an energy sufficient for the escape of neutral atmospheric particles via a cascade of elastic collisions with the background atmospheric gas, a phenomenon that corresponds to escape owing to atmospheric sputtering.

The effect of the Sun on the upper atmospheres of terrestrial planets by means of absorption of UV radiation and atmospheric sputtering by solar-wind plasma results in the production of an extended neutral corona populated with suprathermal atoms of hydrogen, carbon, and oxygen (see Fig. 4). In turn, the hot corona causes changes in the flow of solar-wind plasma at exosphere altitudes, an effect that has an impact on the long-period evolution of the planet's atmosphere itself. Therefore, suprathermal H, C, and O atoms are important components of extended neutral coronas, a fact that is to be taken into account in analyzing evolution processes and investigating the space that surrounds the planet.

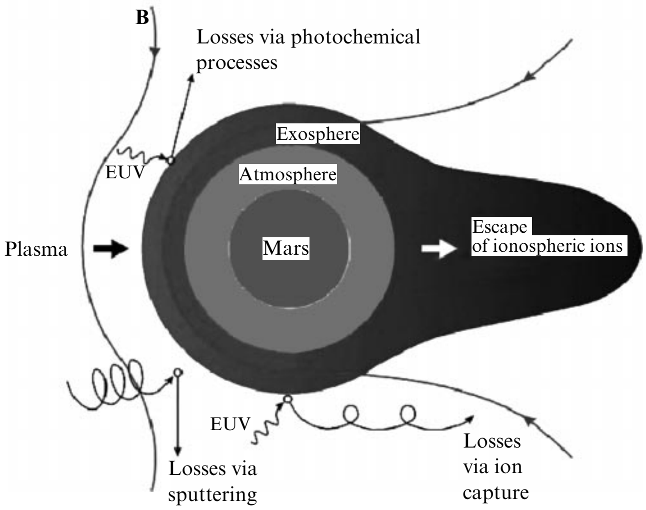

Figure 4. Interaction of solar EUV radiation and solar-wind plasma with the atmosphere/ionosphere of Mars.

4.1 Suprathermal fractions of hydrogen, carbon, and oxygen atoms in the upper atmospheres of Mars and Venus

Kinetic Monte Carlo models intended for studying distributions of suprathermal hydrogen and oxygen atoms in the coronas of Mars and Venus are presented in a sufficiently comprehensive way in [26, 56, 83–86]. In these models, elastic, inelastic, and super-elastic (de-excitation of metastable excitation levels) collisions of suprathermal hydrogen and oxygen atoms with the atmospheric gas are considered; the models also involve differential cross sections that determine scattering angles in those processes. An important part of the numerical model under development is photochemical and plasma sources of suprathermal atoms, such as dissociation of hydrogen and oxygen molecules by solar UV radiation and the accompanying flow of photoelectrons, dissociative recombination of molecular ions, and exothermic ion–molecular reactions and charge exchange of hydrogen atoms with solar-wind protons at exospheric altitudes.

The exothermic ion–molecular reactions and, especially, dissociative recombination of molecular oxygen ions are the most important sources of suprathermal oxygen atoms in the upper atmospheres of terrestrial planets [27, 53, 87]. A major set of photochemical reactions responsible for producing suprathermal oxygen was studied in [88, 89]. We extended that set of exothermic reactions used in the aforementioned models with a refined scheme of channels and energy yields of the reaction of dissociative recombination of the O_2^+ molecular ion:

$$O_2^+ + e \to \begin{cases} O(^3P) + O(^3P) + 6.99\ \text{eV}\,, \\ O(^3P) + O(^1D) + 5.02\ \text{eV}\,, \\ O(^1D) + O(^1D) + 3.06\ \text{eV}\,, \\ O(^1D) + O(^1S) + 0.84\ \text{eV}\,. \end{cases} \tag{18}$$

Oxygen atoms are mainly produced in the ground ^{3}P and metastable ^{1}D and ^{1}S electron states with the respective kinetic energy excesses 6.99, 5.02, 3.06, and 0.84 eV for the reactions channels listed above. The energy yields are calculated under the assumption that the oxygen ions are in the ground vibrational state. The respective probabilities of channels (18) were taken to be 0.22, 0.42, 0.31, and 0.05, using the measurement data from [90].

Sputtering of magnetospheric electrons with high kinetic energies and the effect of photoelectrons are accompanied by excitation, dissociation, and ionization of the atmospheric components, and the corresponding processes were included into the set of exothermic photochemistry reactions that we used. In this way, the dissociation and dissociative ionization by electron impact were regarded as additional sources of suprathermal oxygen atoms,

$$\mathrm{O_2}+\mathrm{e}_a \rightarrow \begin{cases} \mathrm{O}(^3\mathrm{P})+\mathrm{O}(^3\mathrm{P},{}^1\mathrm{D},{}^1\mathrm{S}) + \mathrm{e}_a + \Delta E^{\mathrm{dis}}_{\mathrm{O_2}}\,, & (19)\\ \mathrm{O}^+(^4\mathrm{S})+\mathrm{O}(^3\mathrm{P},{}^1\mathrm{D},{}^1\mathrm{S}) + \mathrm{e} + \mathrm{e}_a + \Delta E^{\mathrm{dis-i}}_{\mathrm{O_2}}\,, & (20)\end{cases}$$

which are also produced in the ground ^{3}P state and electronically excited states ^{1}D and ^{1}S with an excess of kinetic energy of the order of several electron-volts. The distributions of the excessive kinetic energy of the oxygen atoms in the process of dissociation ($\Delta E^{\mathrm{dis}}_{\mathrm{O_2}}$) and dissociative ionization ($\Delta E^{\mathrm{dis-i}}_{\mathrm{O_2}}$) of oxygen molecules O_2 by electron impact were estimated using results of measurements [91] and calculations [92]. The cross sections of the dissociation processes were taken from [91, 92].

The interactions of high-energy magnetospheric protons, that precipitate at high latitudes with atmospheric components are accompanied by a transfer of momentum and energy in elastic and inelastic scattering, ionization, and charge exchange and electron capture in collisions with the main atmospheric molecules and atoms. The energetic hydrogen atoms that are produced under proton impact also affect atmospheric components, transferring momentum and energy to them in elastic, inelastic, and ionization processes. The collisional processes that accompany the penetration of high-energy H^+/H protons and hydrogen atoms into the upper atmosphere of terrestrial planets can be represented as

$$\mathrm{H}^+_{\mathrm{f}}(\mathrm{H}_{\mathrm{f}}) + M \rightarrow \begin{cases} \mathrm{H}^+_{\mathrm{f'}}(\mathrm{H}_{\mathrm{f'}}) + M^*\,,\\ \mathrm{H}^+_{\mathrm{f'}}(\mathrm{H}_{\mathrm{f'}}) + M^+ + \mathrm{e}\,,\\ \mathrm{H}_{\mathrm{f'}}(\mathrm{H}^+_{\mathrm{f'}}) + M^+(M) + \mathrm{e}\,,\end{cases}$$

where M denotes the main atmospheric components O_2, CO_2, CO, N_2, and O. Secondary fast hydrogen atoms $\mathrm{H_{f'}}$ and protons $\mathrm{H^+_{f'}}$ produced in charge exchange and ionization iterate the cycle of impact processes presented above. Hence, the precipitation into the atmosphere of magnetospheric protons and/or solar wind protons should be regarded as a cascade process that is accompanied, in particular, by the production of an ever-growing fraction of suprathermal atoms M^* of the atmospheric gas in electronically excited states. This process is known in the literature as sputtering of the atmosphere induced by high-energy ions [93].

To explore the penetration of the high-energy H^+/H flux into the upper atmosphere of Mars and Venus, we used the kinetic Boltzmann equations [94, 95], because these equations describe scattering in elastic, inelastic, and ionization collisions and charge exchange with the surrounding atmospheric gas and transport of the H^+/H flux. An important consequence of the influx of the high-energy protons and hydrogen atoms to the upper atmosphere is that suprathermal oxygen atoms $\mathrm{O_h}$ are produced in elastic and inelastic collisions of the H^+/H flux with atmospheric oxygen $\mathrm{O_{th}}$:

$$\mathrm{H}^+(\mathrm{H}) + \mathrm{O_{th}} \rightarrow \mathrm{H}^+(\mathrm{H}) + \mathrm{O_h}\,. \tag{21}$$

The suprathermal oxygen atoms that move upward populate the corona, and those with the energies exceeding the gravitational binding energy of the planet form the thermal escape flux [54].

The suprathermal oxygen atoms produced in processes (18)–(21) lose excessive kinetic energy in collisions with the background atmospheric gas and are distributed along the altitude in the transition region between the thermosphere and the exosphere [27, 53, 54]. The kinetics and transport of suprathermal oxygen atoms are described by the Boltzmann equation

$$\mathbf{v}\,\frac{\partial}{\partial \mathbf{r}}\,f_{\mathrm{O_h}} + \mathbf{s}\,\frac{\partial}{\partial \mathbf{v}}\,f_{\mathrm{O_h}} = Q_{\mathrm{O_h}}(\mathbf{v}) + \sum_{M=\mathrm{O,\,N_2,\,O_2,\,CO_2,\,CO}} J_{\mathrm{mt}}(f_{\mathrm{O_h}}, f_M)\,, \tag{22}$$

where $f_{\mathrm{O_h}}(\mathbf{r},\mathbf{v})$ and $f_M(\mathbf{r},\mathbf{v})$ are the respective velocity distribution functions of the suprathermal oxygen atoms and surrounding atmosphere species. The left-hand side of Eqn (22) describes transport of suprathermal oxygen atoms in the planetary gravitational field $\mathbf{s}$. The function $Q_{\mathrm{O_h}}$ in the right-hand side of Eqn (22) determines the energy spectrum in the production of suprathermal oxygen atoms in processes (18)–(21). Integrals J_{mt} for elastic and inelastic collisions of suprathermal atoms with atmospheric particles have standard form (7) under the assumptions that the velocity distribution of surrounding atmospheric gas particles corresponds to the locally equilibrium functions of the Maxwell distribution.

The thermalization rate of suprathermal oxygen atoms depends to a significant extent on the cross sections of collisions with the background atmospheric gas. A key aspect of this numerical model is the stochastic interpretation of the distribution of scattering angles of suprathermal oxygen atoms in elastic and inelastic collisions with atmospheric components. We used the results of recent calculations of differential cross sections for elastic and inelastic collisions of suprathermal oxygen atoms with atmospheric atomic oxygen [96] and molecular nitrogen [97].

Similarly, the kinetic Monte Carlo methods developed for the transport and kinetics of high-energy electrons were used to calculate dissociation rates of molecular oxygen in electron impacts in a CO_2-dominant [98] and H_2-dominant [99] atmosphere. The rates of production of suprathermal hydrogen and oxygen atoms under dissociative recombination of molecular ions and exothermic photochemical reactions were calculated using the stochastic model in [26]. This allowed using the known rates of production of suprathermal hydrogen and oxygen atoms in the photochemical and plasma sources listed above for calculating the kinetics and transport of hydrogen and oxygen atoms in the Venusian and Martian transition regions between the thermosphere and the exosphere in a 1D or 3D version of the stochastic model of the planetary corona [41, 83].

The models based on the kinetic Monte Carlo method [26, 27, 53, 54, 56, 83–86, 100] also provided an option to explore the structure of the hot oxygen coronas of Venus, Mars, and Earth, which are produced as a result of an exothermic reaction, dissociative recombination of one of the main ionospheric ions, the ion of molecular oxygen.

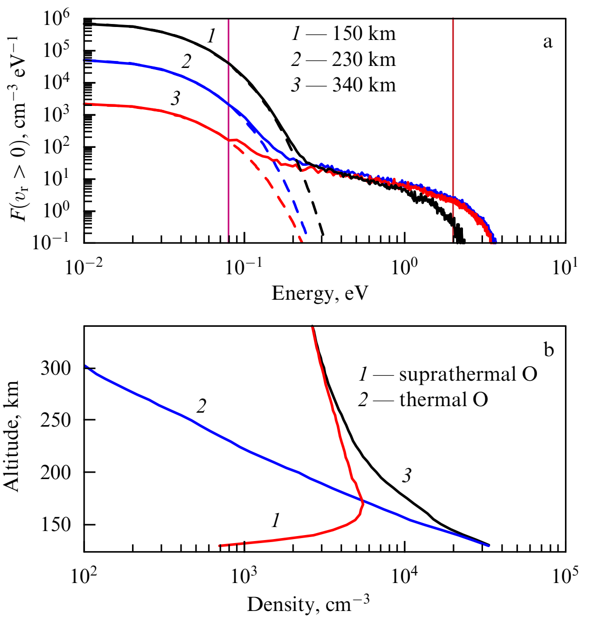

Figure 5. (a) Distribution function of atomic oxygen in the upper atmosphere of Mars at altitudes 150 km (curve *1*), 230 km (curve *2*), and 340 km (curve *3*). Atoms with energies in the region between two vertical lines are those that populate the hot corona. (b) Distribution of oxygen in the corona of Mars: curve *1*, suprathermal atoms; curve *2*, thermal atoms. Curve *3* shows combined distributions *1* and *2*.

Figure 5 shows calculated distributions of suprathermal oxygen atoms in the upper atmosphere of Mars. The kinetic energy distribution of these atoms (Fig. 5a) clearly exhibits the presence of a significant fraction of atoms with suprathermal energies up to 2 eV (the energy of oxygen atom escape from the atmosphere) in comparison with the thermal fraction shown by the dashed line. Local thermal distributions of hydrogen atoms are calculated for the upper atmosphere temperatures 195, 205, and 220 K at the respective altitudes 150, 230, and 240 km [26, 56, 87]. Suprathermal atoms of a photochemical origin populate the hot oxygen corona of Mars (Fig. 5b). Moreover, the reaction of dissociative recombination is currently the main source that causes thermal escape of oxygen atoms from the atmosphere of Mars and hence the loss of significant amounts of water by Mars in the course of its geological evolution.

The rates of production of suprathermal oxygen atoms in the night atmosphere of Venus as a result of dissociative recombination of O_2^+ and NO^+ ions, charge exchange of O^+ ions with the main atmospheric species O, CO_2, and H, as well as radiative recombination of the O^+ ion were first studied in [100]. Figure 6a shows the kinetic energy distribution of the oxygen atoms produced in the night atmosphere of Venus by the photochemical and plasma sources listed above.

Calculations show that dissociative recombination of the O_2^+ ion remains the main source of suprathermal oxygen atoms (Fig. 6a). The altitude profiles (Fig. 6b) of the density of suprathermal oxygen atoms in the night atmosphere of Venus were calculated using the total distribution functions of suprathermal oxygen atoms at an altitude of 160 km (Fig. 6a). It was found that under the conditions of high and moderate solar activity, the concentrations of suprathermal oxygen atoms in the night exosphere are 1 to 2 orders of magnitude smaller than the values characteristic of the day exosphere (Fig. 6b).

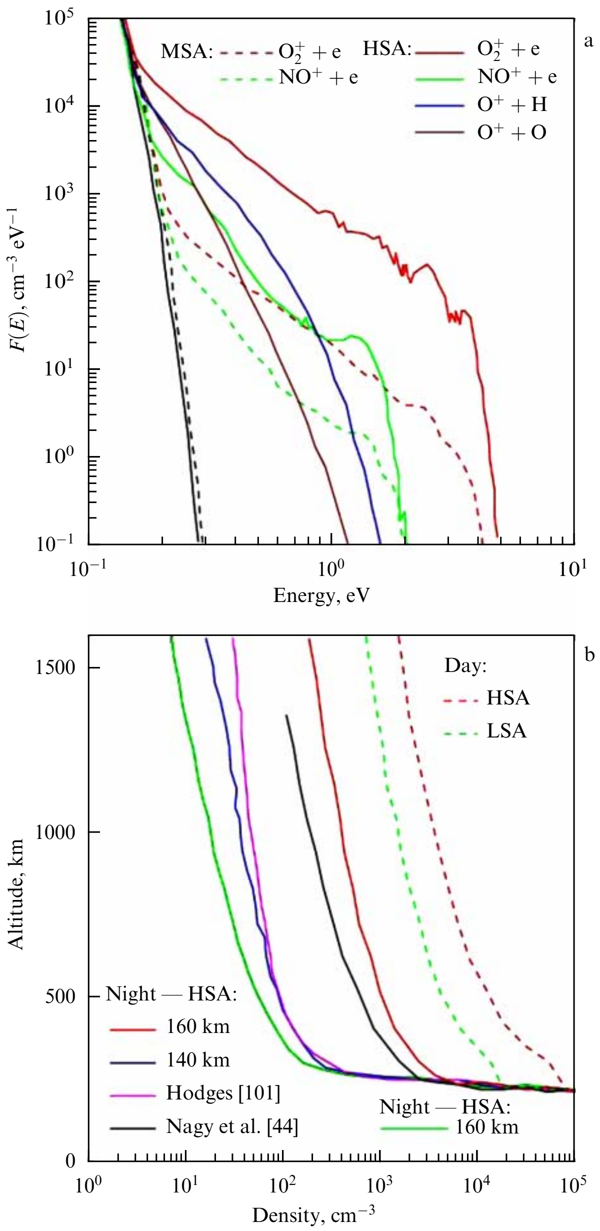

Figure 6. (Color online.) (a) Kinetic energy distribution function of the oxygen atoms at an altitude of 160 km that are produced in the night thermosphere of Venus under the conditions of moderate (MSA) and high (HSA) solar activity. Black color corresponds to local equilibrium distributions: the solid curve for HSA and the broken curve for MSA conditions. (b) Altitude distribution of the density of suprathermal oxygen atoms in the night exosphere of Venus under the conditions of low (LSA), moderate, and high solar activity. Results of calculations in [44, 101] are also shown.

The production of the fraction of suprathermal hydrogen atoms owing to collisions of thermal hydrogen atoms with suprathermal oxygen atoms was also studied [85]. For this, the kinetic Monte Carlo model of a hot oxygen corona [26, 56] was modified by including elastic collisions of atmospheric hydrogen atoms and suprathermal oxygen atoms produced as a result of dissociative recombination of the molecular oxygen ion. This was done based on the general method of the stochastic simulation of the sources, kinetics, and dynamics of suprathermal particles in planetary atmospheres [41]. An important new element of the developed

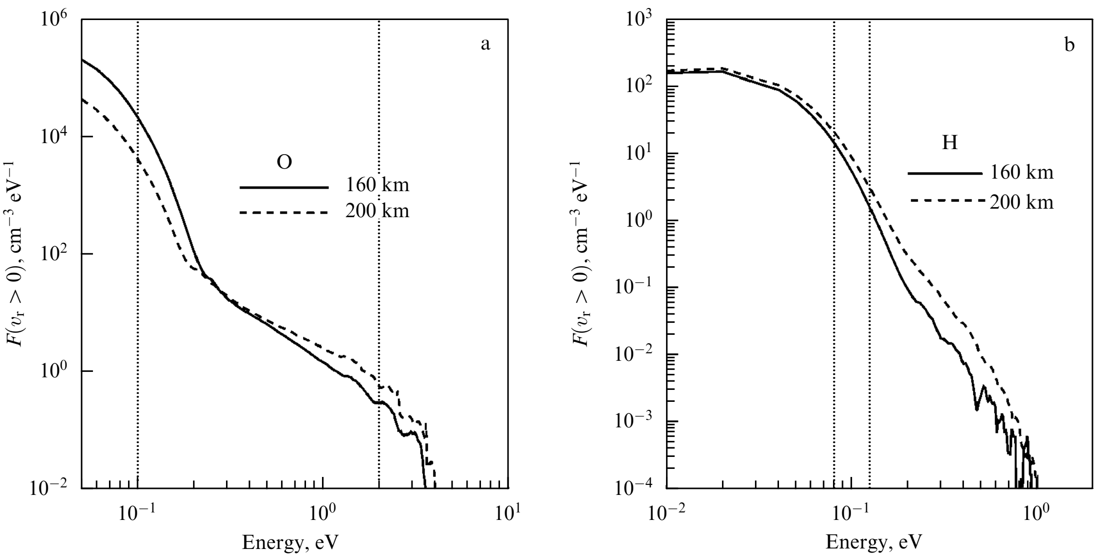

Figure 7. Energy spectra of the distribution function $F(v_r > 0)$ of upward-moving thermal and suprathermal atoms of (a) oxygen and (b) hydrogen at altitudes of 160 and 200 km of the transition region (shown by respective solid and broken curves). The right vertical dotted lines indicate the escape energy of oxygen atoms, ~ 2 eV, and of hydrogen atoms, ~ 0.12 eV, from the atmosphere of Mars, and the left dotted lines indicate the energy $\sim 5T_n \approx 0.08$ eV, the threshold above which oxygen and hydrogen atoms are considered suprathermal.

model is the use of the total and differential cross sections recently calculated in [102] for collisions of hydrogen and oxygen atoms at suprathermal kinetic energies. The differential cross sections of H and O collisions determine the scattering angles in those processes and eventually the efficiency of the transport of excessive kinetic energy from suprathermal oxygen atoms to thermal hydrogen atoms. New data on scattering cross sections have also allowed detailed studies of the kinetics of thermalization of produced suprathermal hydrogen atoms in elastic and inelastic collisions with the main atmospheric species. Because the major part of experimental data on the upper atmosphere and ionosphere of Mars were obtained by the Viking spacecraft in 1976 during the period of a very low solar activity, to make a comparison with the results in [103, 104] with the same initial parameters, only input data that refer to the conditions of low solar activity were used in the calculations presented below.

In numerical implementations of the stochastic model of the hot hydrogen and oxygen corona of Mars, the statistics of distributions of suprathermal hydrogen and oxygen atoms over velocities at all computational cells were accumulated. This allowed assessing local flows of suprathermal oxygen atoms in the transition region of the upper atmosphere of Mars. Figure 7a shows energy spectra of upward-moving suprathermal oxygen atoms at altitudes of 160 and 200 km. The term 'suprathermal particles' is usually applied to those particles whose kinetic energy is 5 to 10 times higher than the average thermal energy. This model considered suprathermal particles with energies over 0.08 eV (this value of kinetic energy is shown by left dotted lines in Figs 7a and 7b; the vertical lines on the right indicate the escape energy for atomic oxygen from the atmosphere of Mars, ~ 2 eV). It can be seen that the range of suprathermal energies less than 2 eV is populated to a significant extent. It is these suprathermal oxygen atoms that form the hot corona.

Calculations show that the hot corona in the area above the exobase consists primarily of suprathermal oxygen atoms of a photochemical origin because, the exosphere is populated with a significant number of such particles owing to transport from lower layers. Hence, in the exosphere, the number of particles whose energy exceeds the escape energy is much larger than at altitudes below the exobase, where the suprathermal particles efficiently thermalize in collisions with atomic oxygen and carbon-dioxide molecules. The calculated estimate of the escape flux of suprathermal hydrogen atoms from the atmosphere under the conditions of low solar activity is 2.3×10^7 cm^{-2} s^{-1}. This value is 30% smaller than the escape flux in the models in [26, 59, 84, 86, 104], which did not take into account the energy transfer from suprathermal oxygen atoms to thermal hydrogen atoms in the transitional area of the upper atmosphere of Mars. Therefore, this value is to be considered more adequate.

Figure 7b shows energy spectra of upward-moving suprathermal hydrogen atoms at altitudes of 160 and 200 km. These atoms gain excessive kinetic energy as a result of momentum and energy transfer in collisions with 'fresh' suprathermal oxygen atoms. Calculations show that this process is an effective source of suprathermal hydrogen atoms in the region of the upper atmosphere of Mars transitional from the thermosphere to the exosphere. Indeed, in the suprathermal energy range, substantial nonequilibrium tails are formed in the kinetic energy distribution of hydrogen atoms. On the other hand, due to the low escape energy of hydrogen atoms from the Martian atmosphere, the population of the suprathermal energy range above 0.12 eV by suprathermal hydrogen atoms is significantly lower than for suprathermal oxygen atoms at altitudes above the exobase. The nonthermal escape flux of hydrogen atoms from the atmosphere due to energy transfer from suprathermal oxygen atoms is estimated to be 6×10^6 cm^{-2} s^{-1} under the conditions of low solar activity.

4.2 Generation of suprathermal hydrogen and oxygen atoms under the effect of solar-wind plasma on the upper atmospheres of Venus and Mars

Nonthermal processes that are initiated by the effect of both solar UV radiation and solar-wind plasma are accompanied by an intensive energy exchange between different degrees of freedom of atmospheric particles and a significant thermal effect of photochemical reactions. The first studies of the interaction of solar wind with Mars were conducted by the Mars-2, Mars-3, and Mars-5 spacecraft as early as the 1970s. The plasma flows in the induced magnetospheric tail were found to primarily consist of oxygen ions, and the first estimates of atmospheric losses, $\sim 1 \times 10^{25}$ ions per second, related to the interaction between the solar wind and the Martian magnetosphere, were obtained (see, e.g., review [105]). Studies of energy transfer in the systems comprising the solar wind, the ionosphere, and the neutral atmosphere of Mars, which were conducted later using the Mars Express, Venus Express, and MAVEN spacecraft, allowed concluding that, a significant number of supra- and superthermal oxygen atoms are produced in the upper atmosphere of these planets [106–108].

To study the distributions of thermal and suprathermal fractions of atomic oxygen in the upper atmosphere of Mars and Venus, a kinetic Monte Carlo model was developed to consider the production of the suprathermal oxygen atom fraction in collisions of oxygen atoms with protons and hydrogen atoms with high kinetic energies that precipitate from the solar-wind plasma. For this, a source of fresh suprathermal oxygen atoms due to precipitation processes was added to the kinetic Monte Carlo model of a hot oxygen corona [26, 56]; that source was included based on the general methodology of stochastic simulation of sources and the kinetics and dynamics of suprathermal particles in planetary atmospheres [41]. We note that the contribution from precipitation was studied previously as a source of supra- and superthermal oxygen atoms for the polar upper atmosphere of Earth [54]. An important next step was the refinement and improvement of the models by comparing their results with measurements of the UV luminosity of atomic hydrogen, carbon, and oxygen in the upper atmospheres of Mars and Venus obtained by the Mars Express, MAVEN, and Venus Express spacecraft [109–111].

The effect of solar-wind plasma on the upper atmosphere of Mars, in combination with photochemical sources created by absorption of soft X-ray and hard ultraviolet solar radiation (see, e.g., [3, 84]), results in the production of an extended neutral corona populated with suprathermal H, C, N, and O atoms. Indeed, one of the first results from the MAVEN spacecraft was the confirmation, using observations made with IUVS (Imaging UV Spectrograph), of the existence of an extended corona consisting of hydrogen, carbon, and oxygen atoms [106, 112]. The hot corona in turn changes under the effect of the influx of solar-wind plasma and local flows to the planetary exosphere of the ions captured in the ionosphere. This influx results in the production of superthermal atoms (energetic neutral atoms, ENAs) escaping from the Martian neutral atmosphere as a result of charge exchange in interactions with precipitating ions with high kinetic energies.

The important role of the effects of solar-wind protons on the upper atmosphere of Mars and Venus is determined by a charge exchange that results in the production of hydrogen and oxygen atoms with both suprathermal ($E \leqslant 10$ eV) and superthermal ($E \geqslant 100$ eV) energies. This is the essence of the main difference between plasma sources and photochemical ones. The above-mentioned Monte Carlo model for solving the kinetic equation, which is intended for studying the role of plasma sources, describes the transport and kinetics of protons and hydrogen atoms (H/H^+) with high energies ($E \leqslant 10$ keV) taking the induced effect of the magnetic field of the solar wind into account. In the kinetic Boltzmann equations for the kinetic energy distributions for H/H^+, the following aspects were taken into account:

— the source of the protons that precipitate at exospheric altitudes into the planet's atmosphere. As a source, the model uses the energy spectra and flows of downward-moving protons at altitudes of 400–500 km, which were measured using ASPERA-3 and ASPERA-4 devices aboard the Mars Express and Venus Express spacecraft;

— the production of high-energy secondary H/H^+ particles in the processes of charge exchange, ionization, and elastic and inelastic scattering with the main atmospheric species. Calculations of the kinetics of those collisions take all available laboratory measurements and theoretical estimates of differential scattering cross sections into account;

— the effect of the induced magnetic field on the motion of protons in the upper atmosphere. The strength of the induced magnetic field on Mars was chosen in accordance with the results of measurements made by the Mars Global Surveyor spacecraft [113] and Mars Express spacecraft [114].

It was assumed in the numerical model that the main component of the magnetic field is horizontal, and hence the depth of proton penetration into the upper atmosphere is limited by the value of the proton gyroradius. The most important part of the model is the stochastic approach to the playout of the scattering angle in the above-mentioned collisions of high-energy protons and hydrogen atoms with the main atmospheric species. The distribution scattering angles in collisions of high-energy H/H^+ measured in laboratory experiments exhibit extremely high peaks in the small-angle region, a feature that largely determines both the efficiency of absorption of proton energy by the atmosphere in collisions and the rate of production of the (backward) flow of protons and hydrogen atoms scattered by the atmosphere. The calculations were done for the range of altitudes 80–500 km, where the lower bound refers to the area of efficient thermalization of high-energy H/H^+ particles in elastic collisions with atmospheric atoms and molecules, and the upper bound is in the region of virtually free molecular flow of H/H^+ and atmospheric particles.

Calculations of the upward flows of protons and hydrogen atoms in the upper atmosphere of Mars under the conditions of minimum solar activity [95] were compared with the results of measurements of those flows made by ASPERA-3 aboard the Mars Express spacecraft. As a boundary condition, the energy spectrum of high-energy protons precipitating into the atmosphere of Mars was used; it was measured at altitudes of 355–437 km in the energy interval 700 eV to 20 keV. The precipitation spectrum is shown in Fig. 8 with a dotted line. The spectrum of downward moving protons used in the calculations corresponds to the energy and particle flows 1.4×10^{-2} erg cm^{-2} s^{-1} and 3.0×10^{6} cm^{-2} s^{-1}. It was found for the first time in calculations that 22% of the particle flow and 12% of the energy flow of the precipitating protons are scattered back into the exosphere (Fig. 8a).

A critical role in transporting charged particles and hence in determining the rate of absorption of solar-wind energy by the upper atmosphere of Mars is played by the induced magnetic field. Calculations have shown that if a horizontal magnetic field with a strength of 20 nT is taken into account, this value being typical according to measurements made by

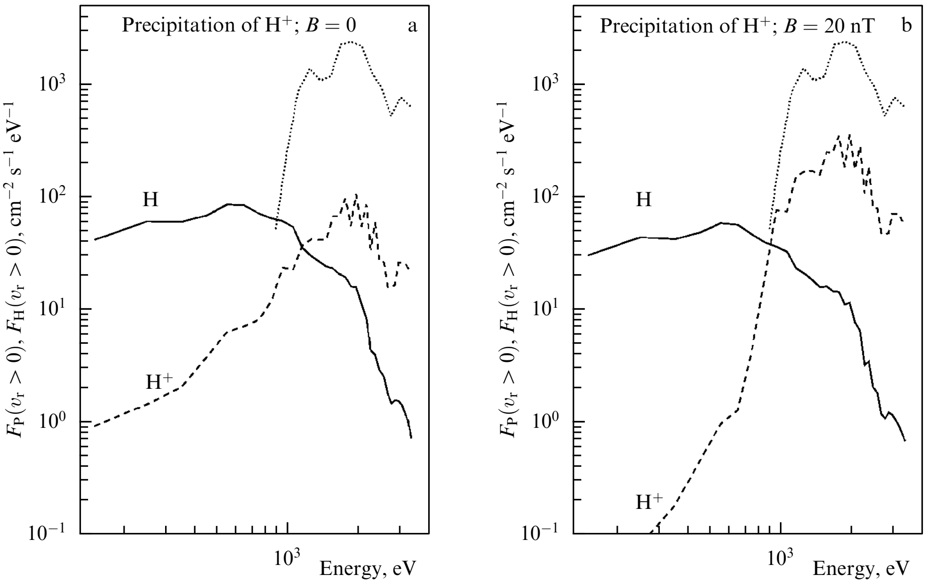

Figure 8. Flows of precipitating protons (dotted line) and those scattered back by the atmosphere (dashed line) and hydrogen atoms (solid curve) at an altitude of 434 km in the upper atmosphere of Mars not taking the induced magnetic field into consideration. (b) Same flows taking the horizontal magnetic field with a strength of 20 nT into consideration.

the Mars Global Surveyor spacecraft [112] and Mars Express [114], then up to 40–50% of the energy flux, depending on the form of the energy spectra of precipitating particles, is scattered back (Fig. 8b).

The upper atmospheres of Mars and Venus are strongly affected by He^{2+} alpha particles from the solar-wind plasma, because charge exchange results in the production of helium atoms and ions, i.e., in changing the helium balance in the planet's atmosphere. To study this process, we developed a Monte Carlo model [115] for solving the kinetic equitation that describes the transport and kinetics of alpha particles and helium ions and atoms ($He/He^+/He^{2+}$) with high energies ($E \leqslant 10$ keV) in the upper atmospheres of terrestrial planets taking the magnetic field induced by the effect of solar wind into account. In the kinetic Boltzmann equations for the kinetic energy distribution function of $He/He^+/He^{2+}$, a source of alpha particles precipitating at exospheric altitudes into the planetary atmosphere was taken into account; as the source, we used the energy spectra and fluxes of downward-moving alpha particles measured using ASPERA-3 and ASPERA-4 aboard the Mars Express and Venus Express spacecraft at altitudes of 400–500 km. An important component of the numerical model is the stochastic approach to playing out the scattering angle in the above-mentioned collisions of high-energy $He/He^+/He^{2+}$ particles with the main atmospheric species. A database was created that includes all available laboratory and theoretical data on total and differential cross sections in collisions with main atmospheric species of high-energy $He/He^+/He^{2+}$ particles. The calculations were done for a range of altitudes from 80 to 500 km, the lower bound corresponding to the region of efficient thermalization of high-energy $He/He^+/He^{2+}$ particles in elastic collisions with atmospheric atoms and molecules, and the upper bound corresponding to the region of virtually free molecular motion of $He/He^+/He^{2+}$ and atmospheric particles.

The calculations of the upward-directed flows of helium atoms and ions in the upper atmosphere of Mars were made for minimum solar activity [115]. As a boundary condition, we used the energy spectrum of high-energy alpha particles precipitating into the atmosphere of Mars, which was measured by the ASPERA-3 instrument at altitudes lower than 500 km in the energy interval from 70 eV to 20 keV. The spectrum of downward moving alpha particles used in the calculations corresponds to the energy and particle fluxes 9.5×10^{-3} erg cm^{-2} s^{-1} and 1.5×10^6 cm^{-2} s^{-1}. In those calculations, it was found for the first time that in the absence of an induced magnetic field, the precipitating flux of alpha particles is not scattered back, i.e., the atoms are assimilated by the atmosphere. If the horizontal magnetic field with a strength of 20 nT is taken into account, up to 30–40% of the energy flux of precipitating alpha particles are scattered back into the planet's exosphere.

The ASPERA-4 device aboard the Venus Express spacecraft recorded only a few cases of precipitation of protons and alpha particles in the atmosphere of Venus. The kinetic Monte Carlo model adapted for Venus [95, 115] was used to determine the fluxes of the particles scattered back by the atmosphere of Venus. As the input parameters, the spectra of protons (the spectrum of proton precipitation adopted in calculations is shown in Fig. 9 with a dotted line) and alpha particles measured by ASPERA-4 were used. The calculations in [116] showed that in the upper atmosphere of Venus under conditions of minimum solar activity, only an insignificant number of the protons (1.9% of the particle flux and 1.3% of the energy flux of precipitating particles) (Fig. 9a) and alpha particles ($< 0.01\%$, below the accuracy of calculations) are scattered back to the exosphere according to the model that does not take the induced magnetic field into account. The obtained results show that the denser atmospheric gas of Venus, unlike the upper atmosphere of Mars, virtually completely assimilates the flux of protons and alpha particles precipitating from the solar wind. If the model takes the horizontal magnetic field with the strength $B = 20$ nT into account (a characteristic value according to measurements by Venus Express), the flux scattered back by the atmosphere significantly increases: up to 44% of the energy flux in the case of precipitating protons (Fig. 9b) and up to

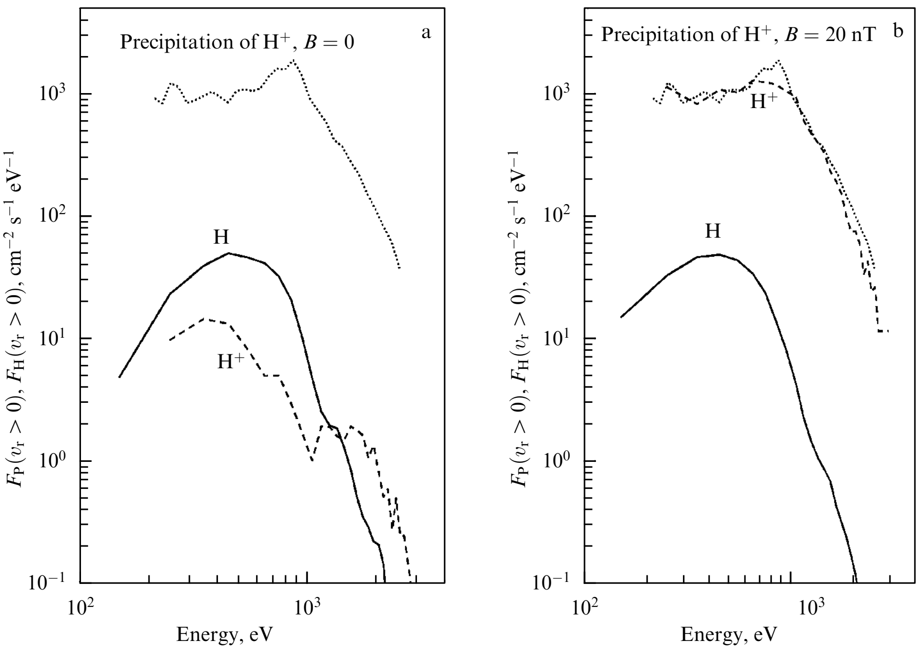

Figure 9. Energy spectra of the precipitating flux (dotted line is for the spectrum measured by the ASPERA-4 instrument) and the upward moving flux (broken curve) of protons and hydrogen atoms (solid curve) (a) without and (b) with the induced magnetic field $B = 20$ nT taken into account.

64% for precipitating alpha particles [116]. For $B = 40$ nT, the flow of backward-scattered energy increases to virtually 100% for both protons and alpha particles. Hence, also in the case of Venus, the induced magnetic field plays a crucial role in transporting charged particles and therefore determines the rate of absorption of solar-wind energy by the upper atmosphere, thus essentially restricting the effect of solar-wind plasma on the planet's thermosphere and ionosphere.

We note that the obtained estimates of the energy flux of precipitating protons scattered back by the atmosphere are smaller than the values found by other authors [117]. This difference in estimated values may be explained by the fact that the Monte Carlo model that we use involves laboratory-measured sets of cross sections and distributions of scattering angles for each collision process, while in previous studies, the hard-sphere approximation was used. It is well known that the hard sphere approximation yields an isotropic distribution of scattering angles, which results in a higher rate of collisional scattering of the precipitating flows of protons and hydrogen atoms in the planetary atmosphere [83, 94, 104].

4.3 Contribution of suprathermal particles to nonthermal dissipation of the extended coronas of Mars and Venus

The kinetic Monte Carlo model was used to study the rate of escape of suprathermal C and O atoms from the present-day Martian atmosphere under the conditions of low and high solar activity [56, 84–86]. The model includes a number of photo- and plasma-chemical sources of suprathermal C and O atoms, such as dissociative recombination of O_2^+, CO_2^+, CO^+, and NO^+ molecular ions, photo and electronic impact dissociation of the main molecules, and exothermic photochemical reactions. The motion of these particles through the upper layers of the atmosphere was studied using the stochastic simulation method [41]. The model included the initial energy distribution of the produced suprathermal atoms and elastic, inelastic, and superelastic (de-excitation) collisions between suprathermal atoms and colder atmospheric gas. Total and energy-dependent differential cross sections were used to determine collision rates and distributions of scattering angles for the collisions listed above.

According to modern data on the neutral atmosphere of Mars [104] adopted as initial parameters of the model, the calculated exobase under the conditions of low and high solar activity is located at the respective altitude of approximately 220 and 260 km above the surface of Mars. The computed functions of the kinetic energy distribution of suprathermal H, C, and O atoms near the exobase (see Section 4.1) were used to calculate nonthermal escape fluxes and density profiles of suprathermal atoms in the exosphere of Mars using kinetic Monte Carlo models [41, 83].

The calculated density profiles of suprathermal oxygen atoms in the atmosphere of Mars, calculated using the energy distribution functions of suprathermal oxygen atoms near the exobase under the conditions of low and high solar activity, are presented in Fig. 10. We can see that for both levels of solar activity, the exosphere density is primarily determined by dissociative recombination of O_2^+ and CO_2^+ molecular ions, resulting in the escape flux of oxygen atoms from the present-day atmosphere of Mars of about 3×10^7 cm^{-2} s^{-1} and the total loss rate about 3×10^{25} s^{-1}. For comparison, the escape rate of oxygen atoms owing to dissociative recombination of CO_2^+ ions ranges from 1.0×10^{25} s^{-1} to 0.9×10^{25} s^{-1} for the same levels of solar activity. We note that the contribution from dissociative recombination of CO_2^+ ions was usually considered to be insignificant and, in most earlier studies of the photochemical escape of oxygen atoms, it was not taken into account, in disagreement with the actual situation. We also note that using energy-dependent total and differential cross sections in our study and taking the elastic, inelastic, and super-elastic collisions at suprathermal energies into account results in exospheric densities of oxygen atoms lower than in studies by other authors (see a review of previous work in [118]).

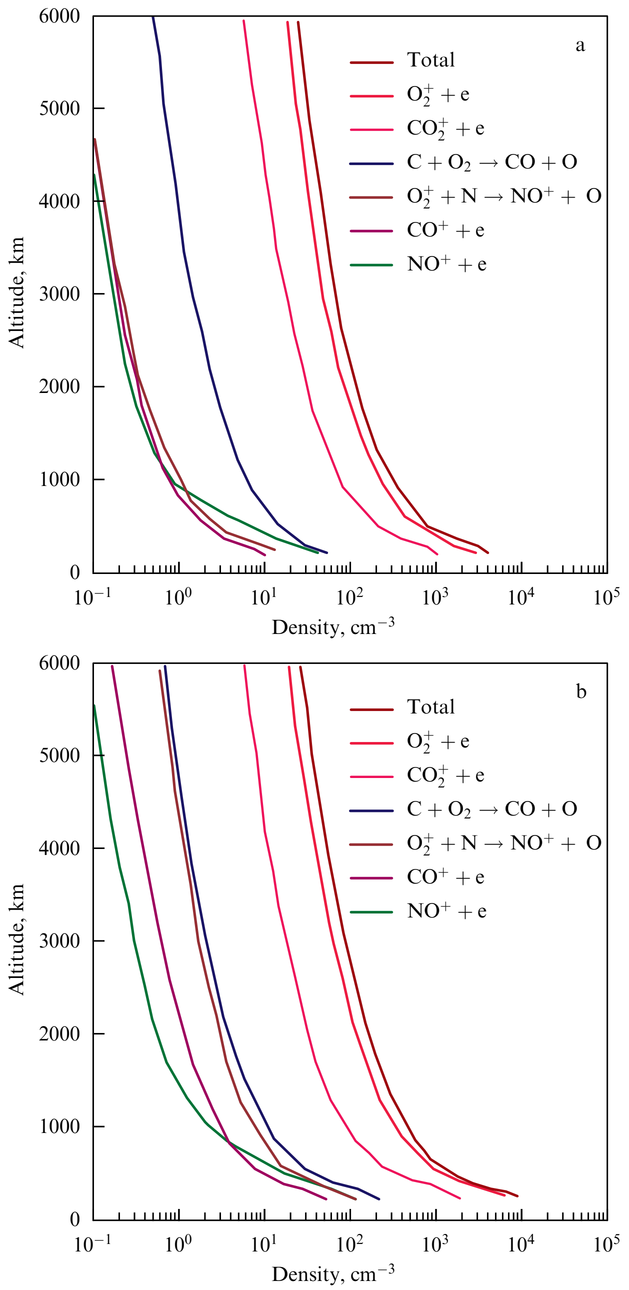

Figure 10. (Color online.) Altitude profiles of the distribution of suprathermal oxygen atoms in the exosphere of Mars for a (a) low and (b) high level of solar activity. Different colored curves show contributions of the reactions of dissociative recombination of molecular ions O_2^+, CO_2^+, CO^+, and NO^+ and exothermic photochemical reactions [84].

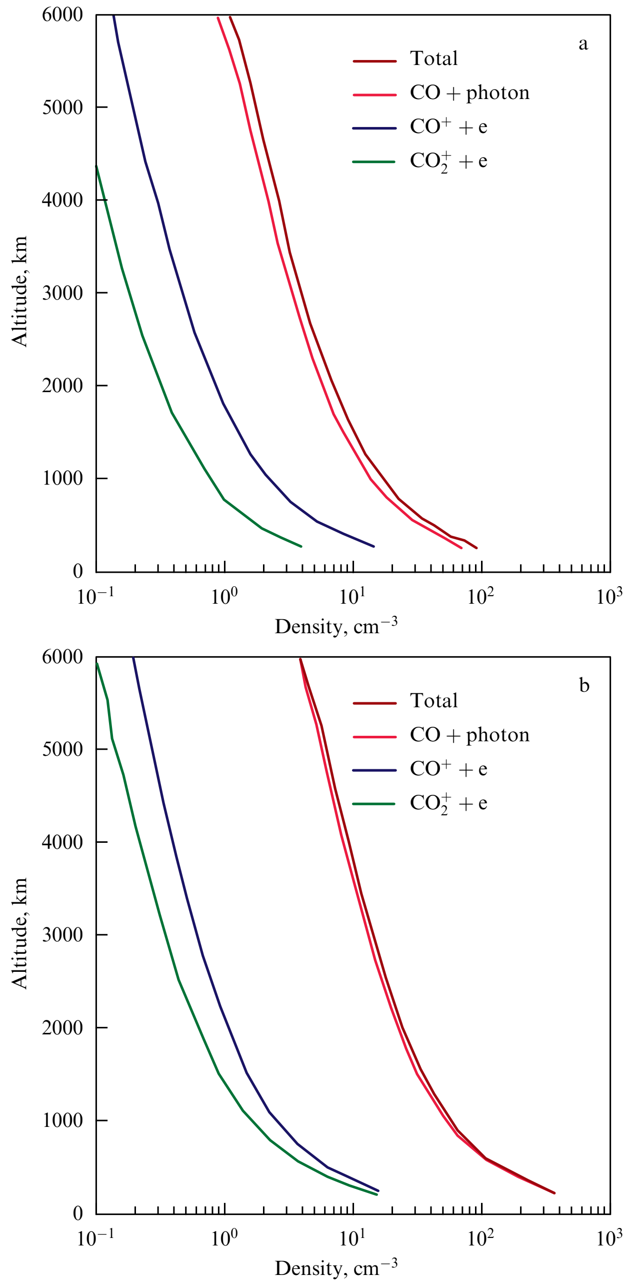

Figure 11. (Color online.) Altitude profiles of the distribution of suprathermal carbon atoms in the exosphere of Mars for a (a) low and (b) high level of solar activity. Different colored curves show the contributions of the reactions of dissociative recombination of molecular ions CO_2^+ and CO^+ and photo dissociation of CO [84].

The exospheric density profiles of suprathermal carbon atoms for the considered sources of suprathermal carbon for low and high solar activity are presented in Fig. 11. Calculations show that currently the main channel for losing atomic carbon from the atmosphere of Mars is photo dissociation of CO, in line with previous studies [48, 119]. The loss fluxes of carbon atoms are about 0.9×10^6 and 3.5×10^6 cm^{-2} s^{-1}, and total losses of carbon are about 0.8×10^{24} and 3.2×10^{24} s^{-1} for the respective low and high levels of solar activity. The values obtained are ~ 5 to 15 times larger than the average rate of atmospheric sputtering of carbon atoms [120] and ~ 35 times larger than the estimated loss rate of molecular ion CO_2^+ that follow from the measurements made by ASPERA-3 [121]. These results show that the escape of suprathermal carbon atoms produced photochemically (by photo and electronic impact dissociation of CO_2 and CO) is the most efficient process of losses of the CO_2-dominant Martian atmosphere at the present time. Thus, exothermic reactions may have played an important role in the dissipation of the Martian atmosphere beginning from Mars's early times. We note that the performed simulation of the suprathermal fractions of C and O atoms and corresponding losses of CO_2 molecules from the atmosphere of Mars depends on the complicated interactions among many physical and chemical processes, for example, variations in the solar radiation flux in the ranges of soft X-ray and

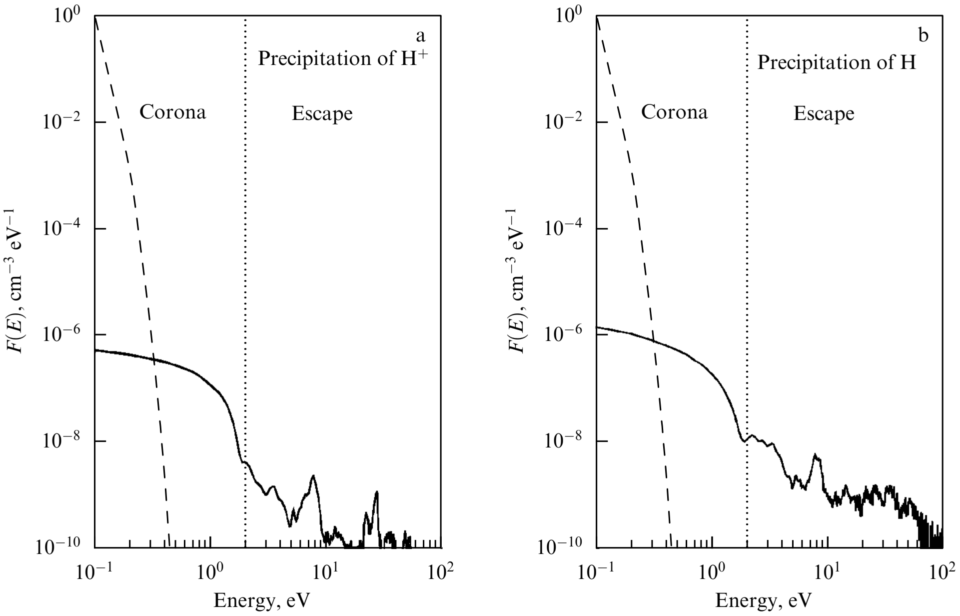

Figure 12. (a) Energy distribution functions (EDFs) of oxygen atoms for the energy spectra [95] of (a) protons and (b) hydrogen atoms that penetrate into the atmosphere of Mars from the solar wind (for protons, measurements made by ASPERA-3) with the horizontal field strength component $B = 10$ nT of the induced magnetic field. EDF shows the spectra of upward-moving oxygen atoms that cross the boundary at an altitude of 400 km. The energy ranges of the atom fractions that populate the hot corona and escape from the atmosphere and the thermal fraction of oxygen corona (dashed lines for an exosphere temperature of 170 K) are indicated. The vertical line indicates the energy of escape of O atoms from the atmosphere of Mars.

extreme ultraviolet radiation and the corresponding response of the upper neutral and ionized atmosphere. Therefore, the present-day rates of atmosphere loss cannot be straightforwardly extrapolated to earlier epochs in the planet's history.

One of the first unexpected results of the MAVEN space mission was the observations, made by the SWIA (Solar Wind Ion Analyzer) instrument, of a low-density population of protons with energies close to the solar-wind energy but at altitudes of the order of 150–250 km in the atmosphere of Mars [122]. Although the penetration of solar wind protons to smaller altitudes is no longer a fully unexpected result in view of the earlier observations made by the Mars Express spacecraft, the velocity of that population virtually corresponds to the observed velocity of the solar wind. From previous studies, it was known that some fractions of the solar wind can interact with the extended corona of Mars. After charge exchange with neutral particles in that corona, some of the protons in the interacting solar wind can capture electrons to become energetic neutral hydrogen atoms. Such neutral particles easily penetrate through the Martian magnetosphere and get into collisional regions of the neutral atmosphere (see, e.g., [95]).

In relation to this, we considered the production, kinetics, and transport of suprathermal oxygen atoms in the transition region (from the thermosphere to the exosphere) of the Martian upper atmosphere in the process of precipitation of high-energy protons and hydrogen atoms. As a source, we used collisions (21) with the transfer of momentum and energy from the flow of precipitating H/H^+ particles with high kinetic energies to atomic oxygen:

$$Q_{O_h} : H^+[H](E) + O_{th}$$

$$\to H^+[H](E' < E) + O_{sth}(E'' = E - E'),$$

meaning that these collisions are accompanied by the production of suprathermal oxygen atoms O_{sth}. This source of suprathermal oxygen atoms was included into kinetic Boltzmann equation (22), whose solution was obtained using the kinetic Monte Carlo model [85, 95, 115]. This approach enabled us to calculate the kinetic-energy distribution function of supra- and superthermal (ENAs) oxygen atoms that are produced in the upper layers of the Martian atmosphere as a result of precipitation of high-energy protons and hydrogen atoms. As the input parameter, we used the flows and energy spectra of precipitating protons that were measured by the ASPERA-3 device under the conditions of a quiet Sun. Those input parameters are described in detail in [85]. The calculated distribution functions of suprathermal hydrogen atoms produced in the precipitation of high-energy protons are shown in Fig. 12.

The calculations showed that the energy distribution functions of oxygen atoms have an essentially nonequilibrium character compared to those of the thermal fraction of the oxygen corona owing to the presence of a significant fraction of oxygen atoms in the range of suprathermal energies (> 0.4 eV). Those functions enable estimating the rates of nonthermal escape of neutral oxygen from the upper Martian atmosphere. Namely, based on studies [84–86], a conclusion was made that the nonthermal escape flow of O atoms due to exothermic photochemical reactions is in the range $(2.5-3.1) \times 10^7$ cm^{-2} s^{-1}, depending on the level of solar activity. At the same time, the escape flux of O atoms due to the precipitation of protons and hydrogen atoms from the solar wind proved to be significantly smaller: it is in the range $(0.7-3.0) \times 10^5$ cm^{-2} c^{-1} for the spectra of precipitating protons measured by the ASPERA-3 device aboard the Mars Express spacecraft under the conditions of low solar activity. However, preliminary results of the measurements made by SWIA aboard the MAVEN spacecraft [122] show that in the case of high solar activity and especially solar bursts, the spectra of the protons penetrating into the atmosphere are more extended in the kinetic energy range, and the values of the differential fluxes can be several orders of magnitude higher than those measured by the ASPERA-3 instrument aboard the Mars Express spacecraft under the conditions of low solar activity. This may explain the high-energy population of protons according to [122].

The upper atmosphere of Mars is known to be subject to not only a regular flux of solar-wind plasma but also an intensive flux of hydrogen atoms with high kinetic energies [123]. In the interaction of solar wind with the exosphere of Mars, energetic hydrogen atoms are produced in a charge exchange of solar wind processes and thermal hydrogen atoms in the corona of Mars. In our calculations, we used two spectra of the hydrogen-atom flux penetrating into the Martian atmosphere at an altitude of 500 km as follows from the results of a hybrid simulation of the interaction of solar-wind plasma with the exosphere of Mars [124, 125]. We used the stochastic model to calculate the kinetic energy distributions of suprathermal oxygen atoms and local fluxes of suprathermal oxygen atoms in the transition region of the upper atmosphere of Mars, shown in Fig. 13.

We found that the exosphere is populated with a significant number of suprathermal oxygen atoms with kinetic energies up to the escape energy, 2 eV, meaning that a hot oxygen corona of Mars is under formation. The energy transfer from the hydrogen atoms precipitating from the solar-wind plasma to thermal oxygen atoms results in the production of an additional nonthermal escape flux of atomic oxygen from the atmosphere of Mars. The escape flux of oxygen atoms induced by precipitation can become dominant in extreme solar events, solar bursts, and coronal mass ejections, as recent observations made by the MAVEN spacecraft showed [126].

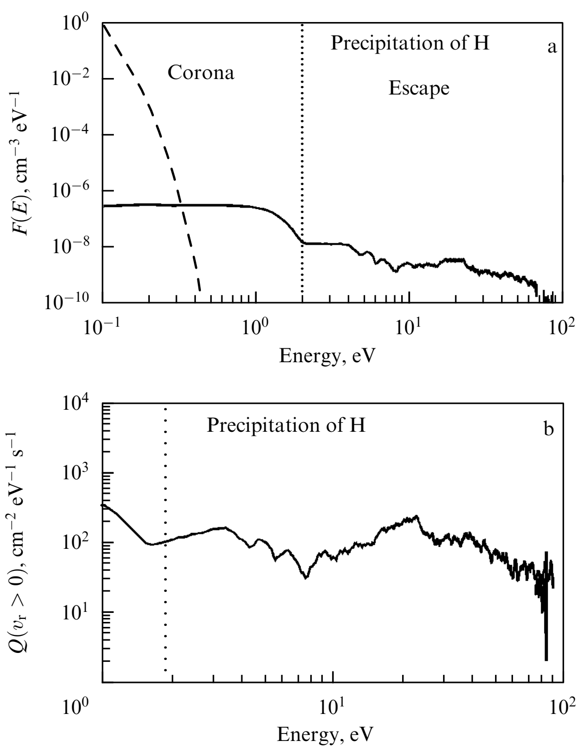

Figure 13. Results of calculations done using the spectrum of precipitating hydrogen atoms (taken from [24]). (a) The kinetic energy distribution functions of upward-moving thermal and suprathermal oxygen atoms at an altitude of 500 km in the atmosphere of Mars are shown with the respective dashed curve (for the exosphere temperature 170 K) and solid curves. The vertical line shows the energy of escape ($\sim$ 2 eV) of oxygen atoms from the atmosphere of Mars. (b) The range in the oxygen atom spectrum that is responsible for forming the escape flow from the atmosphere of Mars owing to precipitation of high-energy hydrogen atoms from the solar-wind plasma.

The results obtained are of significant importance because the MAVEN spacecraft focusing on exploration of atmospheric dissipation is currently in the atmosphere of Mars. Apparently, the dissipation of the upper atmosphere of Mars due to precipitation of fluxes of high-energy protons and hydrogen atoms during solar bursts can become a dominant process as Mars loses its atmosphere on a geological time scale. Accordingly, it becomes possible to compare the calculated rates of nonthermal losses of hydrogen, carbon, and oxygen atoms from the Martian atmosphere with the expected observational data on thermal and nonthermal dissipation of the upper atmosphere of Mars and thus to make important conclusions about the key processes that govern the changes in the climate and atmosphere of Mars in the course of its evolution.

5. Dissipation of the atmospheres of exoplanets

One of the most significant achievements in space studies during the last decade is the discovery of exoplanets and extrasolar planetary systems. Observations of such systems using ground-based and space telescopes operating in the IR and UV wave ranges enable obtaining first estimates of such very important characteristics of the atmospheres of planets in extrasolar planetary systems as the composition and thermal state. Currently, the production, stability, and evolution of the atmospheres of exoplanets are under active exploration using both observations with ground-based and space telescopes and mathematical simulation. A number of important results regarding the nature of the exoplanets have been obtained, and unique specific features were discovered in the planetary systems of single and binary stars that contain bodies substantially different from Solar System planets such as hot Jupiters. In essence, a new area of astrophysics, exoplanetology, that has drastically changed classic planetology, has begun.

Unfortunately, there are no reliable results yet regarding the role of atmospheric dissipation in the evolution of exoplanets. Shortly after observations of the extended hydrogen cloud surrounding a giant exoplanet, transit hot Jupiter HD 209458b [127], several research teams independently developed models [11, 12, 31, 128–132] to study escape in the hydrodynamic regime from atmospheres of hot Jupiters. Despite differences in the details, all of the models satisfactorily agree with the observations of the gaseous hydrogen envelop of the planet but did not allow studying the history of a close-in exoplanet at large time intervals. The problem is primarily related to significant uncertainties in the factors involved in the models, such as the stellar energy flow in the extreme UV range, efficiency of heating (conversion of the absorbed energy of photons into heat), geometric factors (areas of absorption of stellar photons by atmospheric gases), the contribution of heavy elements, etc. Similarly to the impossibility of using time reversal to study the evolution of planets in the early Solar System, including dissipation of atmospheres of terrestrial planets, it is not possible to find the sources of the formation of the atmosphere of a specific exoplanet; however, we can compare specific features of approximately similar planets that are at different stages of evolution [4].

5.1 Losses of hydrogen-dominated atmospheres

A key factor that determines the state of an exoplanet atmosphere is the heating of the atmosphere by radiation from the star. It is of utmost importance for hot Jupiters, i.e., the giant planets orbiting close to the host star ($<$ 0.1 a.u.). After the discovery of the first planets of that type, it was found that the atmospheres of some of those planets extend beyond the Roche lobe, resulting in a strong gas-dynamic outflow of matter from the atmosphere. The hydrogen-dominated upper atmosphere is heated as a result of absorption of the host star's XUV radiation in the range 1–100 nm. This radiation is predominantly absorbed in ionization of atomic hydrogen and helium and ionization, dissociation, and dissociative ionization of molecular hydrogen. Consequently, the efficiency of heating is defined as a ratio of the total rate of local heating of the atmospheric gas and the rate of absorption of the stellar radiation energy. As we have seen, this parameter plays an important role in thermal dissociation of the upper atmospheres of Solar System planets. It is of even greater importance for close-in exoplanets that are subject to strong fluxes of stellar radiation in the extreme UV and soft X-ray ranges. For example, calculations of the heating efficiency in [36, 133] by extreme UV stellar radiation of gas giant HD 209458b, whose upper atmosphere consists primarily of atomic and molecular hydrogen, yielded absorption rates of the energy of the extreme UV radiation flux from the host star and the accompanying flux of primary photoelectrons owing to collisions in the transitional $H_2 \rightarrow H$ area of the upper atmosphere of the planet.

In [36, 133, 134], changes were studied that occur in the temperature distribution of the primordial atmosphere enriched with molecular hydrogen under the effect of a strong flux of solar/stellar XUV radiation. The high rates of ionization and photochemical reactions are shown to eventually result in heating, subsequent expansion of the upper layers of the atmosphere, and the production of suprathermal atoms that can also affect the energy balance in the planet's thermosphere (Fig. 14).

As follows from [36, 133], the efficiency of heating the hydrogen-dominant upper atmosphere of a planet by extreme UV radiation is not over 0.2 at thermosphere altitudes if the effect of photoelectrons is taken into account. The heating-efficiency profiles obtained for the solar spectrum with the radiation flow enhanced by factors of 10 and 100 in the soft X-ray range (1–10 nm) was shown to not differ significantly from the efficiency profile for the standard solar spectrum [133]. Therefore, the calculated heating efficiency can also be used for stars younger than the Sun after scaling the photon flux in the soft X-ray and extreme UV ranges in accordance with the observed stellar spectra. This observation opens the way to obtaining estimated rates of atmosphere outflow for planets of young stars whose spectra differ from that of the Sun.

Depending on the upper atmosphere composition and heating efficiency, the hydrostatic regime of escape can be replaced with the hydrodynamic one. To study this problem, a 1D self-consistent model of the atmosphere of a hot Jupiter was developed [134] that includes three main modules: Monte Carlo, chemical kinetic, and gas-dynamic. The Monte Carlo module uses the Boltzmann equation to calculate the rate of heating of the atmosphere, rates of photoreactions (ionization, dissociation, and dissociative ionization of atmospheric species), and the rates of reactions induced by suprathermal photoelectrons [99, 133]. The rates of photochemical reactions found in the Monte Carlo module are used in the chemical kinetics module to solve the system of chemical kinetics equations [133] and calculate concentrations of atmospheric species in each cell. In the gas-dynamic module, profiles of macroscopic parameters of the atmosphere (density, velocity, and temperature) are calculated. In the atmosphere heating function, the contribution of photoelectrons is taken into account. Because a 1D model was used, the 3D Roche potential had to be approximated by setting it equal to the gravitational potential along the line that connects the centers of the planet and the star.

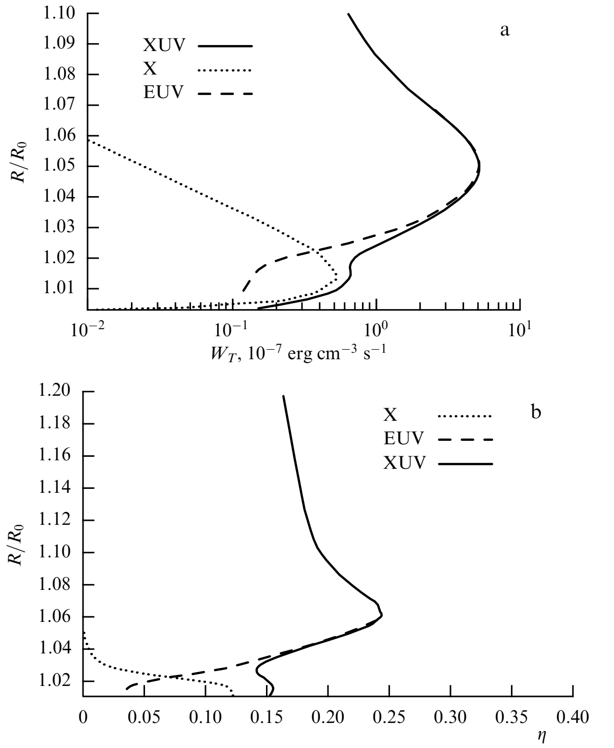

Figure 14. Intensity profile of heating the atmosphere of hot Jupiter HD 209458b by radiation from the star calculated for the solar spectrum and, separately, for X-ray (X) and extreme UV (XUV) ranges. The dotted curve shows the intensity of heating by X-ray radiation, and the dashed curve the intensity of heating by extreme UV radiation (EUV). The solid curve shows the intensity of heating with the complete solar XUV spectrum for exoplanet HD 209458b orbiting at a distance of 0.045 a.u. from the host star. (b) Total efficiency of heating for the base XUV model (solid curve) and its components, the EUV model (dashed curve), and the X model (soft X-ray range) (dotted curve) [133].

We simulated the atmosphere of planet HD 209458b taking the simplified Roche potential into consideration and studied the effect of reactions that involve suprathermal photoelectrons on the dynamics, change in chemical compositions, and rate of outflow of the hydrogen–helium atmosphere of hot Jupiter HD 209458b [135]. The calculations were done for two models, with (M+) and without (M$-$) consideration of photoelectrons, and the results compared with those obtained by other authors. The calculations show that significant differences for models M+ and M$-$ are observed in density profiles. While the velocities of gas

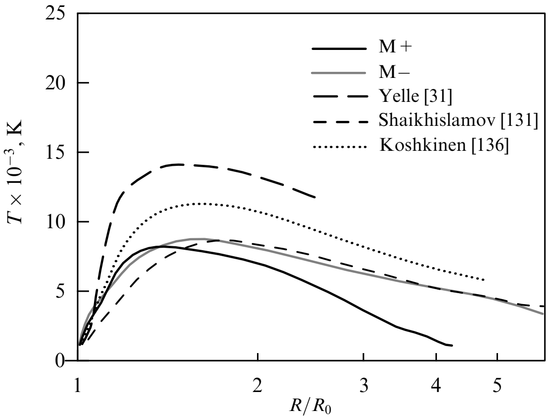

Figure 15. Radial temperature profiles of the atmosphere of hot Jupiter HD 209458b in models with (M+) and without (M−) consideration of the kinetics and transport of photoelectrons [134]. Results of calculations in the gas-dynamic models [31, 131, 136] are also shown.

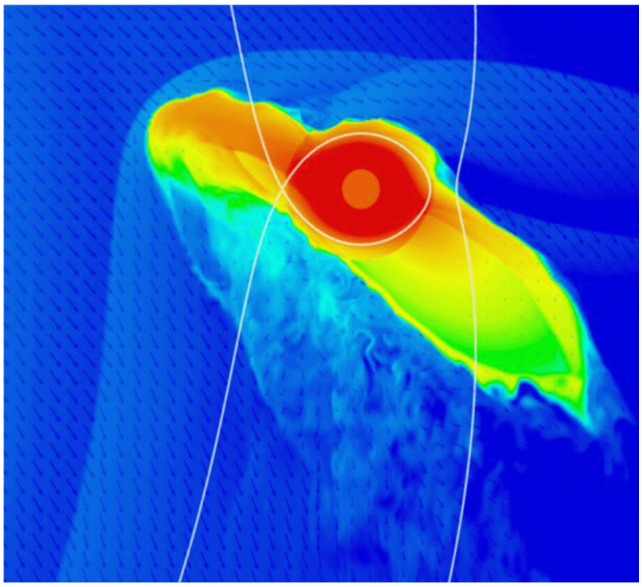

Figure 16. Gas envelope of planet HD 209458b becoming, according to simulation results, essentially asymmetric under the effect of the star's gravitational field and interaction with impinging stellar wind [137].

beyond the Lagrange point L_1 (4.5 planet radii) are virtually the same for both models, the densities are significantly different. This difference results in a difference in the temperature of the atmospheric gas (Fig. 15) and hence in the rate of its loss.

We note that in the models in [11, 136], the atmosphere-heating efficiency was not calculated but was introduced as an external fitting parameter of the model, set at a value above 0.4, which yielded substantially higher temperatures of the upper atmosphere of the exoplanet under study. The calculations also yielded the atmospheric loss rate, which enabled comparison with observational data and calculations by other authors; namely: (a) the estimate $\sim 10^{10}$ g s^{-1} [127] obtained from the analysis of observations by the Hubble space telescope (HST); (b) results of hydrodynamic models, 4×10^{10} g s^{-1} [136], and, 7×10^{10} g s^{-1} [131]; and (c) our calculations of the hydrodynamic-outflow rate of the atmosphere: 4×10^{10} g s^{-1} in model M− and 8×10^9 g s^{-1} in model M+. Despite differences in details (completeness of the physical model, numerical solution methods, the main atmospheric species assumed, and chemical complexity of the environment), all of these models satisfactorily agree with the observations of the hydrogen cloud surrounding hot Jupiter HD 209458b. From the perspective of evolution, of utmost interest is the fact that the model rates of hydrogen losses coincide with each other up to a factor of the order of unity.

It was shown recently in [137] that the regime and rate of atmospheric outflow are determined not only by the state of the exoplanet's atmosphere but also by stellar wind parameters. Therefore, the obtained parameters of the atmosphere can be used as boundary conditions for 3D gas-dynamic calculations that simulate the interaction of the planet's atmosphere with the stellar wind. For example, an interpretation of the HST [127] observation of the extended hydrogen atmosphere of HD 209458b made using a 3D gas-dynamic model of the stellar wind effect on the hydrogen atmosphere [137] shows that, depending on the location of the front collision point, all gas envelopes around hot Jupiters can be divided into two classes:

(1) if the front-collision point is located inside the planet's Roche lobe, the envelopes have an almost spherical form specific to a classical atmosphere, somewhat distorted by the effect of the star and interaction with the stellar wind gas;

(2) if the front-collision point is located outside the planet's Roche lobe, outflow begins in the vicinity of Lagrange points L_1 and L_2, and the envelope becomes either closed or unclosed and significantly asymmetric (Fig. 16).

It follows that thermal and nonthermal escape can affect the transition of the planetary upper atmospheres from a hydrostatic regime to a hydrodynamic one. To see this, we have to study the ratio of the incoming stellar XUV energy and the rate of escape from the planet's atmosphere, which determines the escape efficiency. Not only all energy flows converted into a set of atmospheric chemistry processes but also the energies transported within the thermosphere by photoelectrons and secondary electrons must be full taken into account. Consequently, the calculations of heating efficiency, i.e., the ratio of the energy accumulated by the background atmospheric gas in the form of heat to the absorbed energy of stellar XUV photons, become even more complicated [36, 64].

5.2 Contribution of suprathermal hydrogen atoms

As we have seen, owing to the closeness of hot Jupiters to the host star their atmospheres are subject to the effect of intensive flows of plasma and radiation from the star. This results in high temperatures of the upper atmosphere and significant chemical changes in its compositions, and has a significant impact on the character of the planet evolution due to high flows of hydrogen-atom escape from the atmosphere. In the upper regions of the thermosphere, photoionization of atomic hydrogen starts playing the dominant role. Hence, the composition of the upper atmosphere varies with altitude as $H_2 \rightarrow H \rightarrow H^+$, to become an additional factor in forming an extended atmosphere because such a change in the composition is accompanied by an increase in the characteristic scale, the height of the uniform atmosphere. Processes such as photo dissociation, electron impact dissociation, and dissociative ionization are the main source of thermal and suprathermal hydrogen atoms in the transitional $H_2 \rightarrow H$ domain of the exoplanet's hydrogen-dominant atmosphere

[64, 99]. In earlier aeronomic models, these processes were not studied in detail because it was assumed that rapid local thermalization of suprathermal hydrogen atoms occurs in elastic collisions with the background gas. The excessive thermal energy of hydrogen atoms produced in the dissociation of molecular hydrogen is determined using experimental and theoretical distributions. which contain fractions of relatively low hydrogen atoms with kinetic energies in the range 0–1 eV and a peak near the thermal energy and a fraction of fast hydrogen atoms with kinetic energies 1–10 eV and a peak near 4 eV. For suprathermal energies of hydrogen atoms, the efficiency of energy transfer from suprathermal atoms to thermal hydrogen atoms and molecules in elastic collisions is determined by the phase functions of the scattering angle distribution. As follows from experimental and computational data, the phase functions usually have peaks at small scattering angles and relatively large cross sections of elastic scattering. Consequently, the energy transfer efficiency strongly depends on the collision energy. These specific features of the elastic scattering of suprathermal hydrogen atoms on thermal components of H_2, He, and H largely determine parameters of the suprathermal hydrogen fraction in the exoplanet's upper atmosphere.

In the kinetic Monte Carlo model in [99], it was taken into account that hydrogen atoms are produced in dissociation processes with an excess of kinetic energy, and hence their distribution in the transitional $H_2 \to H$ region of the exoplanet's upper atmosphere is found from the solution of the Boltzmann kinetic equation with the photochemical source of suprathermal hydrogen atoms given by dissociation of H_2. The functions of the source of suprathermal hydrogen atoms were determined using the rate of the photolysis of atmospheric gas by XUV radiation from the star and the accompanying flow of electrons.

The numerical model in [99] includes photo processes of absorption of hard XUV radiation from the star by the exoplanet's atmospheric gas, which are accompanied by excitation, dissociation, and ionization of atmospheric species and the production of a flux of photoelectrons with energies sufficient for subsequent excitation and ionization of atomic and molecular hydrogen. To calculate the rates of the photo processes, transport, and collisional kinetics of photoelectrons in the exoplanet's upper atmosphere, the Monte Carlo model from [98] was used, adapted to hydrogen atmospheres. This implementation of the model relied on experimental and computational data for the cross sections and distributions of scattering angles in elastic, inelastic, and ionization collisions of electrons with the main species: H_2, He, and H. The model in [99] for the first time allowed estimating the production rate and energy spectrum of the hydrogen atoms produced with an excessive kinetic energy in the dissociation of H_2 in the upper atmosphere of exoplanet HD 209458b (Fig. 17).

The numerical statistical model of hot planetary corona [4] adapted to the hydrogen atmospheres of close-in exoplanets was used to perform a detailed study of the kinetics and transport of suprathermal hydrogen atoms in the transitional $H_2 \to H$ domain of the extended upper atmosphere of HD 209458b. Calculations of the distribution functions showed [64, 99] that dissociation of molecular hydrogen is accompanied by the production and transport to the uppermost layers of the transitional $H_2 \to H$ region of an ascending flux of suprathermal hydrogen atoms with kinetic energies that exceed the local escape energy. The estimated escape flux is

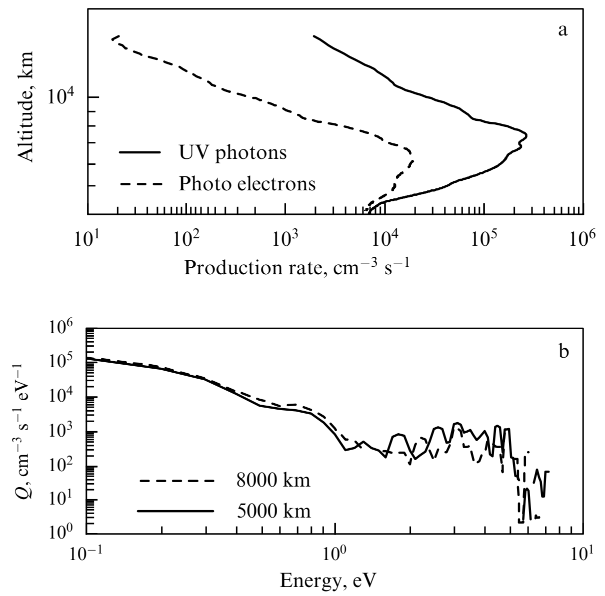

Figure 17. (a) Rate of production of suprathermal hydrogen atoms in the dissociation of molecular hydrogen by XUV photons (solid curve) and photoelectrons (dashed curve) in the upper atmosphere of hot Jupiter HD 209458b. (b) The energy spectrum of the hydrogen atoms produced at an altitude of 5,000 km (solid curve) and 8,000 km (dashed curve) in dissociation and dissociative ionization of H_2 by photoelectrons.

5.8×10^{12} cm^{-2} s^{-1} for a moderate level of stellar activity in the XUV range, which yields the rate of atmospheric losses owing to dissociation of H_2 equal to 5.8×10^9 g s^{-1}. These estimates are close to the estimated $\sim 10^{10}$ g s^{-1} rate of the loss of the HD 209458b atmosphere that follows from observations [127]. Hence, the calculated estimate of the rate of atmospheric loss by this exoplanet can be regarded as a lower bound because the calculations were made for XUV radiation under the conditions of moderate stellar activity. Naturally, in the case of high stellar activity, the contribution of H_2 dissociation by hard XUV radiation of the star and the accompanying flux of photoelectrons in the production of the flux of hydrogen atoms escaping from the atmosphere becomes even more significant. Therefore, this source of suprathermal hydrogen atoms, which is due to the dissociation of H_2, is to be included unto modern aeronomic models of physical and chemical processes in the upper atmospheres of expolanets [64].

It can be expected that future observations will set additional restrictions on the models of dissipation of the exoplanet atmospheres under study to foster progress in planetary aeronomy and a better understanding of the evolution processes, including the formation of an atmosphere and climate on Earth and terrestrial planets in the Solar System.

6. Conclusions

This review, based primarily on studies that have been conducted for many years by the authors, presents kinetic Monte Carlo methods for studying the character and estimating the distributions of suprathermal hydrogen and oxygen atoms in the coronas of terrestrial planets. To describe the rarefied gas of the upper atmosphere, the stochastic method of direct Monte Carlo simulation, equivalent to solving the kinetic Boltzmann equation, was used, which enables reflecting the dynamic and stochastic character of the gas on the molecular level. The models take the most important photochemical and plasma sources of suprathermal atoms into account.

Those models were used to study the rates of production of suprathermal oxygen atoms owing to ion–molecular chemistry reactions and dissociative recombination of molecular ions, charge exchange, and radiative recombination of the atomic oxygen ion in the day and night exospheres of Venus and Mars. It was shown for the first time that under conditions of high and moderate solar activity, the concentrations of suprathermal (hot) oxygen atoms in the night exosphere of Venus are one to two orders of magnitude lower than the values characteristic of day exosphere. For the first time, the rates of production of suprathermal hydrogen atoms that are due to the transport of excessive energy from suprathermal oxygen atoms in collisions with the thermal fraction of atomic hydrogen in the exosphere of Mars were studied. Stationary nonequilibrium functions of the distribution of hydrogen and oxygen atoms in the transition region of the upper atmosphere of Mars were calculated, and the escape rates of H and O atoms were estimated.

The developed models enabled estimating the escape rates of suprathermal oxygen and carbon atoms from the present Martian atmosphere under the conditions of low and high levels of solar activity. The most comprehensive set of possible photo and plasma chemistry sources of suprathermal C and O atoms was taken into account, and the stochastic simulation method was used to study the motion of those particles through the upper layers of the atmosphere. Dissociative recombination of O_2^+ and CO_2^+ molecular ions was shown to be the main source of suprathermal atoms, yielding the rate of atmospheric loss of $(2.5-3.0) \times 10^{25}$ s^{-1} oxygen atoms under conditions of low and high solar activity. It was shown for the first time that the escape rate of oxygen atoms due to dissociative recombination of CO_2^+ ions ranges from 1.0×10^{25} s^{-1} to 0.9×10^{25} s^{-1} for the same levels of solar activity. The nonthermal losses of atomic carbon were shown primarily to be due to photo dissociation of CO with respective rates $(0.8-3.2) \times 10^{24}$ s^{-1} for low and high solar activity. Depending on the solar activity level, the calculated losses of suprathermal carbon atoms proved to be 35 times higher than the losses of CO_2^+ ions, as follows from the recent measurements performed by the ASPERA-3 device aboard the Mars Express spacecraft. The obtained estimated losses of suprathermal carbon and oxygen atoms also exceed the losses of the Martian atmosphere due to atmospheric sputtering by solar-wind plasma and captured ionospheric ions.

The production, kinetics, and transport of suprathermal and superthermal hydrogen and oxygen atoms in the transition region from the thermosphere to the exosphere in the Martian upper atmosphere in the course of sputtering high-energy protons and hydrogen atoms were also studied. The calculations show that the distribution functions of O atoms feature an essentially nonequilibrium character compared to the distribution function of the thermal fraction of the oxygen corona in the range of suprathermal energies (> 0.4 eV). The nonthermal escape flux of O atoms due to exothermic photochemical reactions is known to be in the range $(2.5-3.0) \times 10^7$ cm^{-2} s^{-1}, depending on the solar activity level, while the escape flux of O atoms due to precipitation of protons and hydrogen atoms from the solar wind is significantly smaller, $(0.7-28.0) \times 10^5$ cm^{-2} s^{-1}, for the spectra of precipitating protons under conditions of low solar activity that were measured by ASPERA-3. However, the preliminary data of measurements done by the SWIA instrument aboard the MAVEN spacecraft show that in the case of high solar activity, especially of solar bursts, the kinetic-energy spectra are more extended and the differential fluxes can be several orders of magnitude higher than those measured by the ASPERA-3 instrument under the conditions of low solar activity. Consequently, dissipation of the upper atmosphere of Mars owing to precipitation of the flux of high-energy protons and hydrogen atoms in solar bursts can become the dominant process in the loss of the atmosphere by Mars on a geological time scale.

Nonthermal processes on Mars and Venus were shown to be initiated by not only the effect of solar ultraviolet and soft X-ray radiation but also the plasma of the impinging solar wind accompanied by an intensive energy exchange between different degrees of freedom of atmospheric particles and a significant thermal effect of photochemical reactions that occur in the interaction between the solar wind and the quasimagnetosphere. In calculating the production of the fraction of suprathermal oxygen atoms in collisions of atmospheric oxygen atoms with the protons and hydrogen atoms precipitating with high kinetic energies from the solar wind plasma, the source of 'fresh' suprathermal oxygen atoms effective owing to precipitation was taken into account based on the general methods of stochastic simulation of the sources, kinetics, and dynamics of suprathermal particles in planetary atmospheres. Those models were refined and improved by comparing their results to the measurements of UV luminosity of atomic hydrogen, carbon, and oxygen in the upper atmospheres of Mars and Venus that were made on the Mars Express, MAVEN, and Venus Express spacecraft.

Based on the developed kinetic Monte Carlo model, the energy spectra of the flow of protons and hydrogen atoms with suprathermal energies that are scattered back by the atmosphere of Mars were obtained for the first time. As a boundary condition, we used the energy spectrum of high-energy protons penetrating into the atmosphere of Mars, which were measured by the ASPERA-3 instrument aboard the Mars Express spacecraft at altitudes of 355 to 437 km in an energy interval from 700 eV to 20 keV. It was found that in thee absence of an induced magnetic field, 22% of the particle flow and 12% of the energy flux of precipitating protons are scattered back into the exosphere. It was found for the first time that if the horizontal component of the induced magnetic field with a characteristic strength of 20 nT is taken into account, up to 40–50% of the energy flux of the precipitating protons is scattered back into space around Mars.

Similar calculations were done to study the kinetics precipitation of solar-wind alpha particles (He^{2+} ions) into the upper atmospheres of Mars and Venus. The energy spectra of the fluxes of suprathermal-energy alpha particles, ions, and helium atoms scattered back by the atmosphere of Mars were obtained for the first time. The calculations showed that in the absence of an induced magnetic field, the precipitating flux of alpha particles is not scattered back by the atmosphere. The same results also showed that if the horizontal magnetic field with a characteristic value $B = 20$ nT is taken into account, up to 30–40% of the energy flux of precipitating alpha particles is scattered back into the planet's exosphere. Thus, it was confirmed that the induced magnetic field plays a crucial role in the transport of charged particles and hence determines the rate of solar-wind absorption by the upper atmosphere of Mars. In calculating the precipitation of protons and alpha particles into the neutral atmosphere of Venus, the fluxes of particles scattered back by the atmosphere were also determined. It was found that in the upper atmosphere of Venus in the absence of an induced magnetic field and under conditions of minimum solar activity, only a vanishingly small part of protons and alpha particles is scattered back into the atmosphere. Accounting for the induced field drastically changes the situation: for values of the horizontal magnetic field ~ 20 nT that are measured on Venus, the energy flow scattered back by the atmosphere increases to 44% for precipitating protons and 64% for precipitating alpha particles. For a field up to 40 nT, the scattered-back energy fluxes of protons and alpha particles increase to virtually 100%, i.e., the atmosphere proves to be fully protected against penetration of solar-wind particles.

Studies of distributions of suprathermal hydrogen, carbon, and oxygen atoms that are produced in the upper atmospheres of Mars and Venus are an important basic problem of comparative planetary aeronomy. Studies of energy transfer in the solar-wind–ionosphere– neutral-atmosphere systems of Mars that were conducted by the Mars Express and MAVEN spacecraft confirm the simulation results according to which a significant number of suprathermal (hot) hydrogen, carbon, and oxygen atoms are produced in upper atmospheres of terrestrial planets. Indeed, the solar effect on the upper atmospheres of those planets via absorption of UV radiation and atmospheric sputtering by solar plasma results in the production of a flow of solar-wind plasma at exospheric altitudes that affects the long-period evolution of the atmosphere itself. Hence, suprathermal H, C, and O atoms are important species of the extended neutral coronas, determining thermal and nonthermal dissipation of the atmosphere and being a characteristic feature of space surrounding the planet. Data on thermal and nonthermal dissipation of the upper atmospheres of Mars and Venus enable drawing far-reaching conclusions regarding key processes in the evolution of the terrestrial planets close to Earth and, in this way, possible unfavorable trends in Earth's evolution.

Methods for studying the dissipation of neutral species of the atmospheres of Solar System planets that were developed by the authors of this review enabled using those approaches for studying the production, stability, and evolution of gas envelopes of extrasolar planets (exoplanets).

Of significant interest are model calculations of hydrogen escape from the discovered extended hydrogen cloud surrounding hot Jupiters that occurs in the hydrodynamic regime, because the atmospheres of many of those planets extend beyond the Roche lobe. A 1D self-consistent model of the atmosphere of a hot Jupiter that includes the Monte Carlo module, the chemical kinetics module, and the gas-dynamic module was used to calculate the rate of heating of the atmosphere by photochemical reactions and the profiles of microscopic parameters of the atmosphere in the transition from the hydrostatic flow regime to the hydrodynamic, associated with thermal and nonthermal escape processes. The atmosphere of hot Jupiter HD 209458b was simulated taken the Roche potential into consideration, and the effect of the reactions involving suprathermal photoelectrons on the dynamics, changes in chemical composition, and the rate of outflow of the hydrogen and helium envelope of HD 209458b was determined. The results agree well with the estimates that follow from observations by the Hubble space telescope and the results of other hydrodynamic models. The obtained parameters of the atmosphere can be used as boundary conditions for 3D gas-dynamic calculations that model the interaction of the planet with the stellar wind. The efficiencies of the conversion of stellar radiation into heat in the soft X-ray and extreme UV ranges, which plays an especially important role in ionization, photo chemistry, and thermal dissociation of upper atmospheres of planets subject to an intensive flux of hard radiation, are estimated. It was found that the calculated efficiencies of heating for the solar spectrum can also be used for stars younger than the Sun if the photon flux is scaled in the soft X-ray and extreme UV ranges in accordance with observations of the spectra of stars. This enables estimating the rate of atmospheric outflow for planets of young stars, whose spectra differ from the Sun's spectrum.

Photo ionization and dissociation of H_2 (photo dissociation, electron impact dissociation, dissociative ionization, etc.), the main sources of thermal and suprathermal hydrogen atoms in the upper atmospheres, first and foremost, of hot Jupiters and Neptunes, which were not taken into account in previous aeronomic models of those processes, have been studied in detail. We showed that the efficiency of energy transport highly depends on the energy of elastic collisions, which is small at small scattering angles, and the specific features of the elastic scattering of suprathermal hydrogen atoms on thermal species of H_2, He, and H largely determine, the parameters of the suprathermal hydrogen fraction in the exoplanet's upper atmosphere. In the developed stochastic model, the distribution of hydrogen atoms in the transitional $H_2 \to H$ region of the upper atmosphere is found from a solution of the Boltzmann kinetic equation that includes a photochemical source of suprathermal hydrogen atoms with excessive kinetic energy produced in dissociation of H_2, and the source function of those atoms is determined from the rates of photolysis of the atmospheric gas by UV radiation from the star and the accompanying flux of photoelectrons. The numerical model takes into account that the absorption of the star's extreme UV radiation is accompanied by excitation, dissociation, and ionization of atmospheric species and the production of a flux of photoelectrons with energies sufficient for subsequent excitation and ionization of atomic and molecular hydrogen. To calculate the rates of the photo processes, transport, and collisions kinetics of photoelectrons, a Monte Carlo model adapted to hydrogen atmospheres was used. The developed model enabled for the first time determining the production rate and energy spectrum of the hydrogen atoms produced with an excess of kinetic energy in the dissociation of H_2 in the upper atmosphere of exoplanet HD 209458b and showing that the source of suprathermal hydrogen atoms that is due to dissociation of H_2 is to be included in modern models of physical and chemical processes in the upper atmospheres of exoplanets.

Unfortunately, because of the uncertainty in energy and geometric factors, the calculations failed to clarify the problem of evolution of the exoplanet atmosphere subject to the effect of intensive fluxes of plasma and electromagnetic radiation for close-in exoplanets. Nevertheless, the models enabled setting important bounds on the variety of photochemical processes in planetary atmospheres and, at the same time, creating a basis required for developing dedicated programs of observations of exoplanets using ground-based and space telescopes.

Studies of extrasolar planets make an immense contribution to explaining dissipation of planet atmospheres and, primarily, terrestrial planets in the early Solar System and thus offering an approach to the reconstruction of their formation history. We can expect that the expansion of the research area far beyond the Solar System and further improvement in mathematical models developed on the basis of exoplanet aeronomy will facilitate better understanding of evolution processes and key problems of planetary cosmogony.

Acknowledgements
The work of V I Sh was supported by the Russian Foundation for Basic Research (project 18-02-00721). The joint research of the authors was conducted with financial support from grants by the Russian Foundation for Basic Research 14-02-00319 and 17-02-00507 and as part of the Program of Basic Research of the Presidium of RAS No. 28.

References

1. Marov M Ya, Shematovich V I, Bisicalo D V *Space Sci. Rev.* **76** 1 (1996)
2. Shizgal B D, Arkos G G *Rev. Geophys.* **34** 483 (1996)
3. Johnson R E et al. *Space Sci. Rev.* **139** 355 (2008)
4. Massol H et al. *Space Sci. Rev.* **205** 153 (2016)
5. Lammer H et al. *Mon. Not. R. Astron. Soc.* **439** 3225 (2014)
6. Kasting J F, Pollack J B *Icarus* **53** 479 (1983)
7. Chassefière E *J. Geophys. Res.* **101** 26039 (1996)
8. Chassefière E *Icarus* **126** 229 (1997)
9. Marov M Ya, Grinspoon D H *The Planet Venus* (New Haven: Yale Univ. Press, 1998)
10. Wordsworth R, Pierrehumbert R *Science* **339** 64 (2013)
11. Tian F et al. *Science* **308** 1014 (2005)
12. Erkaev N V et al. *Astrobiology* **13** 1011 (2013)
13. Marov M Ya, Gal'tsev A P, Shari V P *Solar Syst. Res.* **19** 9 (1985); *Astron. Vestn.* **19** 15 (1985)
14. Marov M Ya *The Fundamentals of Modern Astrophysics. A Survey of the Cosmos from the Home Planet to Space Frontiers* (New York: Springer, 2015)
15. Kasting J F *Icarus* **74** 472 (1988)
16. Ramirez R M et al. *Nature Geosci.* **7** 59 (2014)
17. Halevy I, Head J W (III) *Nature Geosci.* **7** 865 (2014)
18. Wordsworth R et al. *Geophys. Res. Lett.* **44** 665 (2017)
19. Marov M Ya *Kosmos. Ot Solnechnoi Sistemy Vglub' Vselennoi* (From Solar System to the Heart of the Universe) (Moscow: Fizmatlit, 2016)
20. Tian F, Kasting J F, Solomon S C *Geophys. Res. Lett.* **36** L02205 (2009)
21. Hunten D M *Planet. Space Sci.* **30** 773 (1982)
22. Marov M Ya, Kolesnichenko A V *Vvedenie v Planetnuyu Aeronomiyu* (An Introduction to Planetary Aeronomy) (Moscow: Nauka, 1987)
23. Chamberlain J W, Hunten D M *Theory of Planetary Atmospheres. An Introduction to Their Physics and Chemistry* (Orlando: Academic Press, 1987)
24. Shematovich V I et al. *J. Geophys. Res.* **108** 5085 (2003)
25. Wayne R P *Chemistry of Atmospheres. An Introduction to the Chemistry of the Atmospheres of Earth, the Planets, and Their Satellites* 2nd ed. (Oxford: Oxford Univ. Press, 1991)
26. Krestyanikova M A, Shematovich V I *Solar Syst. Res.* **40** 384 (2006); *Astron. Vestn.* **40** 418 (2006)
27. Shematovich V I, Bisikalo D V, Gérard J-C *J. Geophys. Res.* **99** 23217 (1994)
28. Bisikalo D V, Shematovich V I, Gérard J-C *J. Geophys. Res.* **100** 3715 (1995)
29. Öpik E J, Singer S F *Phys. Fluids* **4** 221 (1961)
30. Chamberlain J W *Planet. Space Sci.* **11** 901 (1963)
31. Yelle R V *Icarus* **170** 167 (2004)
32. Volkov A N et al. *Astrophys. J. Lett.* **729** L24 (2011)
33. Parker E N *Astrophys. J.* **139** 72 (1964)
34. Watson A J, Donahue T M, Walker J C G *Icarus* **48** 150 (1981)
35. Tian F et al., in *Comparative Climatology of Terrestrial Planets* (Eds S J Mackwell et al.) (Tucson: Univ. of Arizona Press, 2013) p. 567
36. Shematovich V I, Ionov D E, Lammer H *Astron. Astrophys.* **571** A94 (2014)
37. Vidal-Madjar A, Bertaux J L *Planet. Space Sci.* **20** 1147 (1972)
38. Hartle R E *Planet. Space Sci.* **21** 2123 (1973)
39. Kim Y H, Son S, Kim J *J. Korean Astron. Soc.* **34** 25 (2001)
40. De La Haye V et al. *J. Geophys. Res.* **112** A07309 (2007)
41. Shematovich V I *Solar Syst. Res.* **38** 31 (2004); *Astron. Vestn.* **38** 28 (2004)
42. Fox J L, Galand M I, Johnson R E *Space Sci. Rev.* **139** 3 (2008)
43. Nagy A F, Banks P M *J. Geophys. Res.* **75** 6260 (1970)
44. Nagy A F et al. *Geophys. Res. Lett.* **8** 629 (1981)
45. Nagy A F, Cravens T E *Geophys. Res. Lett.* **15** 433 (1988)
46. Nagy A F, Kim J, Cravens T E *Ann. Geophys.* **8** 251 (1990)
47. Kim J et al. *J. Geophys. Res.* **103** 29339 (1998)
48. Nagy A F et al. *J. Geophys. Res.* **106** 21565 (2001)
49. Shizgal B, Lindenfeld M J *Planet. Space Sci.* **27** 1321 (1979)
50. Shizgal B D *J. Gephys. Res.* **104** 14833 (1999)
51. Kabin K, Shizgal B D *J. Geophys. Res.* **107** 5053 (2002)
52. Bird G A *Molecular Gas Dynamics and the Direct Simulation of Gas Flows* (Oxford: Clarendon Press, 1994)
53. Shematovich V et al. *J. Geophys. Res.* **104** 4287 (1999)
54. Shematovich V I, Bisikalo D V, Gérard J-C *Geophys. Res. Lett.* **32** L02105 (2005)
55. Shematovich V I et al. *Icarus* **173** 480 (2005)
56. Krest'yanikova M A, Shematovich V I *Solar Syst. Res.* **39** 22 (2005); *Astron. Vestn.* **39** 26 (2005)
57. Marconi M L, Dagum L, Smyth W H *Astrophys. J.* **469** 393 (1996)
58. Leblanc F, Johnson R E *Planet. Space Sci.* **49** 645 (2001)
59. Valeille A et al. *Icarus* **206** 18 (2010)
60. Michael M, Johnson R E *Planet. Space Sci.* **53** 1510 (2005)
61. Smyth W H, Marconi M L *Icarus* **181** 510 (2006)
62. Combi M R *Icarus* **123** 207 (1996)
63. Bisikalo D V et al. *Astrophys. J.* **798** 21 (2015)
64. Shematovich V I, Bisikalo D V, Ionov D E, in *Characterizing Stellar and Exoplanetary Environments* (Astrophysics and Space Science Library, Vol. 411, Eds H Lammer, M Khodachenko) (Berlin: Springer , 2015) p. 105
65. Marov M Ya, Shematovich V I, Bisikalo D V *Kineticheskoe Modelirovanie Razrezhennogo Gaza v Zadachakh Aeronomii* (Kinetic Simulation of Rarefied Gas in Aeronomy Problems) (Moscow: Keldysh Institute of Applied Mathematics, 1990)
66. Marov M Ya et al. *Nonequilibrium Processes in the Planetary and Cometary Atmospheres: Theory and Applications* (Astrophysics and Space Science Library, Vol. 217) (Dordrecht: Kluwer Acad. Publ., 1997)
67. Ferziger J H, Kaper H G *Mathematical Theory of Transport Processes in Gases* (Amsterdam: North-Holland, 1972); Translated into Rissian: *Matematicheskaya Teoriya Protsessov Perenosa v Gazakh* (Moscow: Mir, 1976)
68. Zmievskaya G I, Pyarnpuu A A, Shematovich V I *Sov. Phys. Dokl.* **24** 692 (1979); *Dokl. Akad. Nauk SSSR* **248** 561 (1979)
69. Shematovich V I et al. *Matem. Mod.* **14** (8) 44 (2002)
70. Shematovich V I, in *Matematicheskie Zadachi Prikladnoi Aeronomii* (Mathematical Problems of Applied Aeronomy) (Ed. M Y Marov) (Moscow: Keldysh Institute of Applied Mathematics, 1987) p. 199
71. Shematovich V I, Bisikalo D V, Gerard J-C, in *Neustoichivye Protsesy vo Vselennoi* (Unstable Processes in the Universe) (Ed. A G Masevich) (Moscow: Kosmosinform, 1994) p. 230
72. Shematovich V *AIP Conf. Proc.* **1084** 1047 (2008)
73. Pyarnpuu A A, Cheredov V V, Shematovich V I *Matem. Mod.* **13**(7) 88 (2001)
74. Stantcheva T, Shematovich V I, Herbst E *Astron. Astrophys.* **391** 1069 (2002)
75. Yanitsky V E *Vesovye Skhemy Statisticheskogo Metoda Chastits v Yacheikakh* (Weight Schemes of the Statistical Particle Models in Cells) (Applied Mathematics Letters) (Moscow: Computer Center of the USSR Academy of Sciences, 1990)
76. Rjasanow S, Wagner W *J. Comput. Phys.* **124** 243 (1996)
77. Leontovich M A *Zh. Eksp. Teor. Fiz.* **5** 211 (1935)

78. Kac M, in *The Boltzmann Equation. Theory and Application* (Eds E G D Cohen, W Thirring) (Vienna: Springer-Verlag, 1973) p. 379
79. Prigogine I *Non-equilibrium Statistical Mechanics* (New York: Interscience Publ., 1962); Translated into Russian: *Neravnovesnaya Statisticheskaya Mekhanika* (Moscow: Mir, 1964)
80. Van Kampen N G *Stochastic Processes in Physics and Chemistry* (Amsterdam: North-Holland); Translated into Russian: *Stokhasticheskie Protsessy v Fizike i Khimii* (Moscow: Vysshaya Shkola, 1990)
81. Ivanov M S, Rogasinsky S V *Sov. J. Numer. Anal. Math. Modell.* **3** 453 (1988)
82. Rjasanow S, Schreiber T, Wagner W *J. Comput. Phys.* **145** 382 (1998)
83. Gröller H et al. *J. Geophys. Res. Planets* **115** E12017 (2010)
84. Gröller H et al. *Planet. Space Sci.* **98** 93 (2014)
85. Shematovich V I *Solar Sys. Res.* **47** 437 (2013); *Astronom. Vestn.* **47** 475 (2013)
86. Shematovich V I, Marov M Ya *Dokl. Phys.* **60** 188 (2015); *Dokl. Ross. Akad. Nauk* **461** 660 (2015)
87. Fox J L *J. Phys. Conf. Ser.* **4** 32 (2005)
88. Hickey M P, Richards P G, Torr D G *J. Geophys. Res.* **100** 17377 (1994)
89. Gérard J-C et al. *Geophys. Res. Lett.* **22** 279 (1995)
90. Kella D et al. *Science* **276** 1530 (1997)
91. Cosby P C *J. Chem. Phys.* **98** 9560 (1993)
92. Van Zyl B, Stephen T M *Phys. Rev. A* **50** 3164 (1994)
93. Johnson R E *Energetic Charged-Particle Interactions with Atmospheres and Surfaces* (Physics and Chemistry in Space, Vol. 19) (New York: Springer-Verlag, 1990)
94. Gérard J-C et al. *J. Geophys. Res.* **105** 15795 (2000)
95. Shematovich V I et al. *J. Geophys. Res.* **116** A11320 (2011)
96. Kharchenko V et al. *J. Geophys. Res.* **105** 24899 (2000)
97. Balakrishnan N, Kharchenko V, Dalgarno A *J. Geophys. Res.* **103** 23393 (1998)
98. Shematovich V I et al. *J. Geophys. Res.* **113** E02011 (2008)
99. Shematovich V I *Solar Syst. Res.* **44** 96 (2010); *Astron. Vestn.* **44** 108 (2010)
100. Gröller H et al. *Geophys. Res. Lett.* **39** L03202 (2012)
101. Hodges R R (Jr.) *J. Geophys. Res.* **105** 6971 (2000)
102. Zhang P et al. *J. Geophys. Res.* **114** A07101 (2009)
103. Kim J et al. *J. Geophys. Res.* **103** 29339 (1998)
104. Fox J L, Hać A B *Icarus* **204** 527 (2009)
105. Vaisberg O *Planet. Space Sci.* **119** 69 (2015)
106. Chaufray J Y et al. *Geophys. Res. Lett.* **42** 9031 (2015)
107. Deighan J et al. *Geophys. Res. Lett.* **42** 9009 (2015)
108. Lee Y et al. *Geophys. Res. Lett.* **42** 9015 (2015)
109. Hubert B et al. *Icarus* **207** 549 (2010)
110. Soret L et al. *Icarus* **264** 398 (2016)
111. Bisikalo D V et al. *Icarus* **282** 127 (2017)
112. Schneider N M et al. *Science* **350** aad0313 (2015)
113. Brain D A et al. *J. Geophys. Res.* **108** 1424 (2003)
114. Akalin F et al. *Icarus* **206** 104 (2010)
115. Shematovich V I et al. *J. Geophys. Res.* **118** 1231 (2013)
116. Shematovich V I et al. *Solar Syst. Res.* **48** 317 (2014); *Astron. Vestn.* **48** 343 (2014)
117. Gunell H et al. *Planet. Space Sci.* **53** 433 (2005)
118. Fox J L, Hac A B *Icarus* **228** 375 (2014)
119. Fox J L *J. Geophys. Res.* **109** A08306 (2004)
120. Chassefière E, Leblanc F, Langlais B *Planet. Space Sci.* **55** 343 (2007)
121. Barabash S et al. *Nature* **450** 650 (2007)
122. Halekas J S et al. *Geophys. Res. Lett.* **42** 8910 (2015)
123. Kallio E, Barabash S *J. Geophys. Res.* **106** 165 (2001)
124. Wang X-D et al. *EPSC Abstracts* **10** EPSC2015-174 (2015)
125. Wang X-D et al. *J. Geophys. Res.* **121** 190 (2016)
126. Jakosky B M et al. *Science* **350** aad0210 (2015)
127. Vidal-Madjar A et al. *Nature* **422** 143 (2003)
128. García Muñoz A *Planet. Space Sci.* **55** 1426 (2007)
129. Murray-Clay R A, Chiang E I, Murray N *Astrophys. J.* **693** 23 (2009)
130. Bisikalo et al. *Astrophys. J.* **764** 19 (2013)
131. Shaikhislamov I F et al. *Astrophys. J.* **795** 132 (2014)
132. Luger R, Barnes R *Astrobiology* **15** 119 (2015)
133. Ionov D E, Shematovich V I *Solar Syst. Res.* **49** 339 (2015); *Astron. Vestn.* **49** 373 (2015)
134. Ionov D E, Shematovich V I, Pavlyuchenkov Ya N *Astron. Rep.* **61** 387 (2017); *Astron. Zh.* **94** 381 (2017)
135. Tsvetkov A G, Shematovich V I *Solar Syst. Res.* **44** 177 (2010); *Astron. Vestn.* **44** 195 (2010)
136. Koskinen T T et al. *Icarus* **226** 1695 (2013)
137. Bisikalo D V et al. *Astron. Rep.* **57** 715 (2013); *Astron. Zh.* **90** 779 (2013)